NASA TECHNICAL NOTE

NASA TN D-6762

c.1

NASA TN D-6762

UPPER-STAGE SPACE-SHUTTLE PROPULSION BY MEANS OF SEPARATE SCRAMJET AND ROCKET ENGINES

by Leo C. Franciscus and John L. Allen

Lewis Research Center
Cleveland, Ohio 44135

NATIONAL AERONAUTICS AND SPACE ADMINISTRATION • WASHINGTON, D. C. • MAY 1972

1. Report No. NASA TN D-6762	2. Government Accession No.	3. Recipient's Catalog No.
4. Title and Subtitle UPPER-STAGE SPACE-SHUTTLE PROPULSION BY MEANS OF SEPARATE SCRAMJET AND ROCKET ENGINES		5. Report Date May 1972
		6. Performing Organization Code
7. Author(s) Leo C. Franciscus and John L. Allen		8. Performing Organization Report No. E-6555
		10. Work Unit No. 139-06
9. Performing Organization Name and Address Lewis Research Center National Aeronautics and Space Administration Cleveland, Ohio 44135		11. Contract or Grant No.
		13. Type of Report and Period Covered Technical Note
12. Sponsoring Agency Name and Address National Aeronautics and Space Administration Washington, D.C. 20546		14. Sponsoring Agency Code
15. Supplementary Notes		

16. Abstract

A preliminary mission study of a reusable vehicle from staging to orbit indicates payload advantages for a dual-propulsion system consisting of separate scramjet and rocket engines. In the analysis the scramjet operated continuously and the initiation of rocket operation was varied. For a stage weight of 227 000 kilograms (500 000 lb), the payload was 10.4 percent of stage weight or 70 percent greater than that of a comparable all-rocket-powered stage. When compared with a reusable two-stage rocket vehicle having a 22 700-kilogram (50 000 lb) payload, the use of the dual propulsion system for the second stage resulted in significant decreases in lift-off weight and empty weight, indicating possible lower hardware costs.

17. Key Words (Suggested by Author(s)) Shuttle orbiter, Second-stage propulsion, Air breathing engines, Dual propulsion system, Scramjet, Rocket, Hypersonic vehicle, Hypersonic engines, Lifting vehicles	18. Distribution Statement Unclassified - unlimited

19. Security Classif. (of this report)	20. Security Classif. (of this page)	21. No. of Pages	22. Price*
Unclassified	Unclassified	51	$3.00

* For sale by the National Technical Information Service, Springfield, Virginia 22151

CONTENTS

UPPER-STAGE SPACE-SHUTTLE PROPULSION BY MEANS OF SEPARATE SCRAMJET AND ROCKET ENGINES

by Leo C. Franciscus and John L. Allen

Lewis Research Center

SUMMARY

A preliminary mission study was made for a propulsion system consisting of a separate scramjet and rocket engines for powering a reusable vehicle from staging to orbit. The merit of the system was defined in terms of the payload delivered to a 500-kilometer (270-n mi) circular orbit. The scramjet and rocket engine sizes, the Mach number for initiating rocket operation, and the flight path were optimized in terms of payload. All-rocket and all-scramjet propulsion were also considered. Stage weight was varied from 136 000 to 454 000 kilograms (300 000 to 1 000 000 lb), and staging Mach numbers were varied from 8 to 12. Estimates of propellant weight fraction and hardware weight of a rocket powered first stage were also made to determine the effects of staging Mach number in terms of lift-off weight and total hardware weight.

The results of the study showed that for a second-stage weight of 227 000 kilograms (500 000 lb), a payload of 10.4 percent of stage weight could be delivered into orbit. This was 70 percent higher than the payload of a rocket second stage of the same stage weight on the same flight path. When compared with a reusable two-stage shuttle-type rocket vehicle having a payload of 22 700 kilograms (50 000 lb), the total weight at lift-off was reduced 56 percent by using scramjet-rocket second-stage propulsion and the empty weight was 42 percent lower than the all-rocket vehicle indicating possible reduced hardware costs. However, the possible consequences on first-stage structural weight and stage separation dynamics at higher dynamic pressures were not investigated. The best staging Mach number was 8 for lowest lift-off weight and highest percent of payload to total hardware weight.

In general, the highest payloads were obtained by (1) delaying rocket-ignition until Mach numbers of about 18 when the acceleration margin provided by the scramjet diminished, (2) using a progressively fuel-rich scramjet equivalence ratio as flight velocity increased, and (3) flying a constant dynamic pressure flight path of 24 kilonewtons per square meter (500 lb/ft^2).

INTRODUCTION

Intensive studies are presently in progress for a reusable, orbital launch vehicle (space shuttle) based on a two-stage rocket-powered, vertical-takeoff, horizontal-landing concept (e.g., refs. 1 to 3). This type of vehicle is based on technology levels suited for initial operation in the late 1970's. Airbreathing engines have not been considered for primary propulsion because their level of development is not considered sufficient for the initial shuttle operation time. A number of studies have investigated airbreathing engines for first-stage propulsion (refs. 4 to 8). In references 7 and 8, for example, an airbreathing first stage plus rocket-powered second stage was studied for a possible second-generation shuttle vehicle. In reference 7, the airbreathing engines were turbojets for acceleration to Mach 3.5 and convertible scramjets from Mach 3.5 to 10, whereas in reference 8, hydrogen-fueled turboramjets were studied.

Thusfar, an airbreathing second stage has been given little consideration for a future-generation shuttle vehicle. In the study of reference 9, a second-stage scramjet-powered vehicle had a higher payload fraction than rocket-powered second stages but was unattractive costwise due to the higher hardware weight. In reference 10, however, a second stage powered by a scramjet-rocket hybrid engine had a higher payload to hardware weight fraction than rocket or scramjet-powered vehicles. Since scramjet engine thrust becomes marginal at high hypersonic speeds, the higher thrust of the hybrid engine resulted in a large decrease in engine size with accompanying reductions in propellant and vehicle structural weights. This result suggests that the selective use of a separate rocket to augment the scramjet at high hypersonic speeds would also reduce the engine size and, in addition, retain the advantages of the high scramjet specific impulse at lower speeds. The purpose of the present study, therefore, was to evaluate a propulsion system consisting of separate hydrogen-fueled scramjets and hydrogen-oxygen rocket engines for powering a second-stage vehicle. Payload, in percent of second-stage gross weight, was used as the figure of merit.

Since the scramjet is an integral part of the vehicle, engine and vehicle performance are closely related. For example, variations in engine size affect the vehicle in terms of aerodynamics, size, and weight. A mission study was performed to evaluate this propulsion system and the effects of vehicle and engine parameters in terms of payload. A flat top, semiconical vehicle configuration was adopted for the study (fig. 1). The stage gross weight was varied between 136 000 and 454 000 kilograms (300 000 to 1 000 000 lb). Vehicle parameters included the fore and aft cone angles and the wing sweep back angle. A number of constant-dynamic-pressure flight paths ranging from 14.4 to 72 kilonewtons per square meter (300 to 1500 lb/ft^2) and staging Mach numbers from 8 to 12 were investigated. Vehicle insulation weight was determined from the time-temperature histories of the flight. The propulsion system consisted of a semicircular annular scramjet with

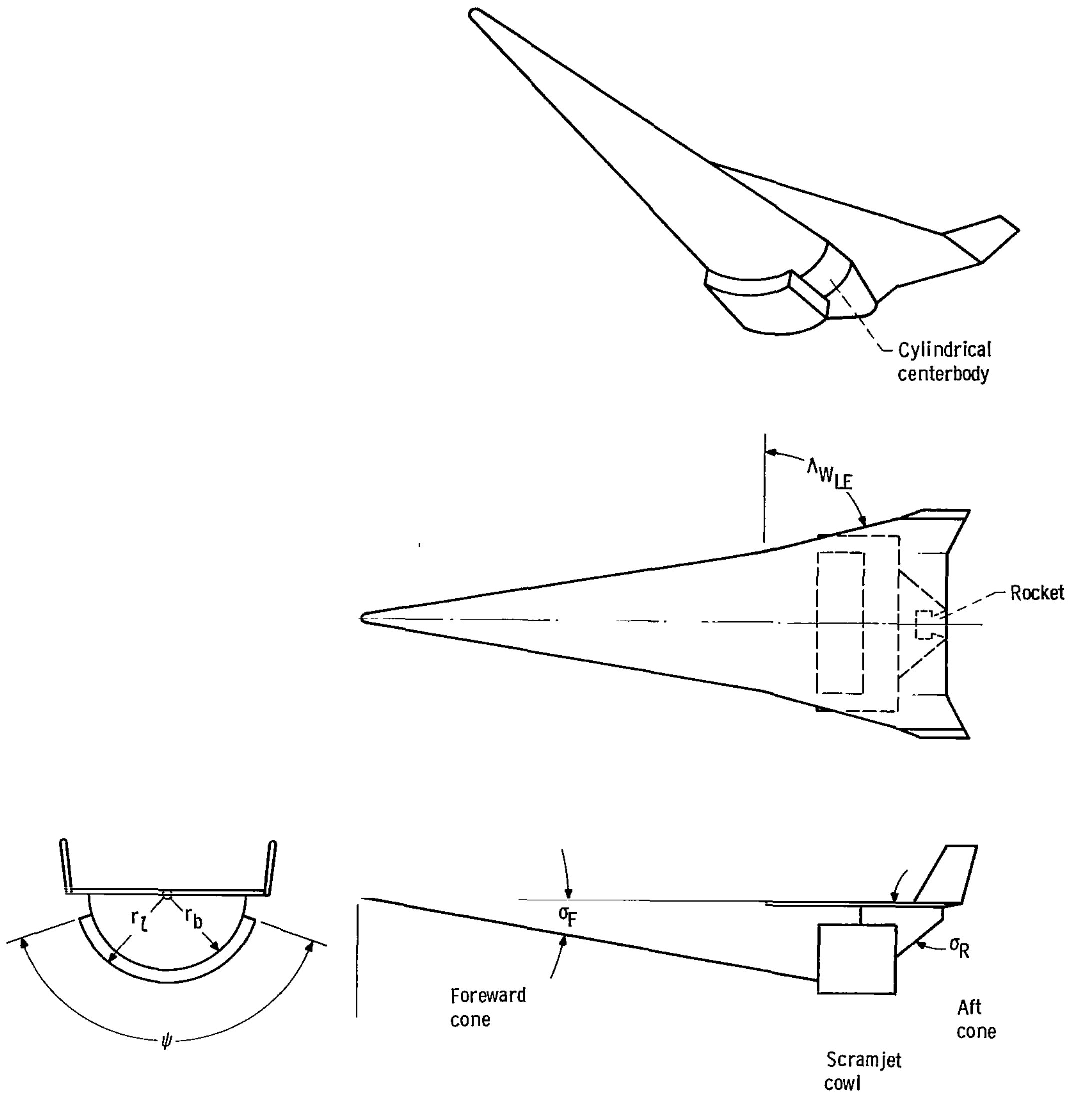

Figure 1. - Vehicle configuration.

the cowl wrapped around the vehicle centerbody and the rocket engine located at the base of the vehicle. The propulsion system parameters included the scramjet cowl central angle, the augmentation ratio defining the relative sizes of scramjet and rocket, and the rocket-on Mach number. The scramjet powers the vehicle from the staging Mach number up to the rocket-on Mach number, after which both scramjet and rocket operate simultaneously until a velocity greater than orbital speed is reached. The vehicle then zooms to the transfer ellipse having a perigee of 83.3 kilometers (54 n mi), an apogee of 185.2 kilometers (99.8 n mi), and an inclination of 55°. Rocket propulsion is used to transfer to a 500-kilometer (270 n-mi) circular orbit.

Each vehicle of specified gross weight and configuration was "flown" over a constant-dynamic-pressure flight path. The calculated propellant weight included that used for acceleration, postorbital maneuvering equivalent to a velocity increment of 457.2 meters per second (1500 ft/sec) and 10 minutes operating time for go-around and landing by turbofan engines. The payload was calculated as the difference between the gross weight and the propellant plus empty weight (structure, engine, and equipment).

METHOD OF ANALYSIS

Vehicle Configuration

Figure 1 shows the flat-top, semiconical vehicle configuration used in the study. Although a more sophisticated vehicle may be required to actually achieve the performance levels presumed herein, the simplicity of this configuration lends itself more easily to airframe aerodynamics and weight estimates. The conical forebody of the vehicle acts as the compressive surface for the air entering the scramjet. The constant-area combustor is located between the cowl and vehicle centerbody. The aft section of the cowl and the vehicle rear cone act as expansion surfaces for the exhaust gas. The rocket engine is located in the base of the vehicle rear cone. The payload package located in the center of the vehicle has a density of 80.1 kilograms per cubic meter (specific gravity = 0.08) and a length to diameter ratio of 4.

Each vehicle configuration was specified by particular values of vehicle parameters (σ_F, σ_R, Λ, etc.) shown in figure 1. (All symbols are defined in appendix A.) The wing and vertical stabilizer taper ratios were fixed at 1/3 and the wing trailing edge sweep angle and vertical stabilizer leading edge sweep angle were fixed at 60°. The vehicle size (length and diameter) was then determined by iteration to provide the volume required for the liquid hydrogen and oxygen, the payload, and the rocket engine. A tank ullage allowance of 10 percent and a body volumeric efficiency of 75 percent were assumed. The best vehicle configuration was then selected by optimizing the configuration parameters in terms of payload.

Flight Path

In order to evaluate the propulsion system considered in this report, the vehicle was "flown" over various constant dynamic pressure q flight paths from the staging Mach number M_S to zoom velocities greater than the orbital velocity of 7867 meters per second (25 800 ft/sec). The zoom velocities include 235 meters per second (770 ft/sec),

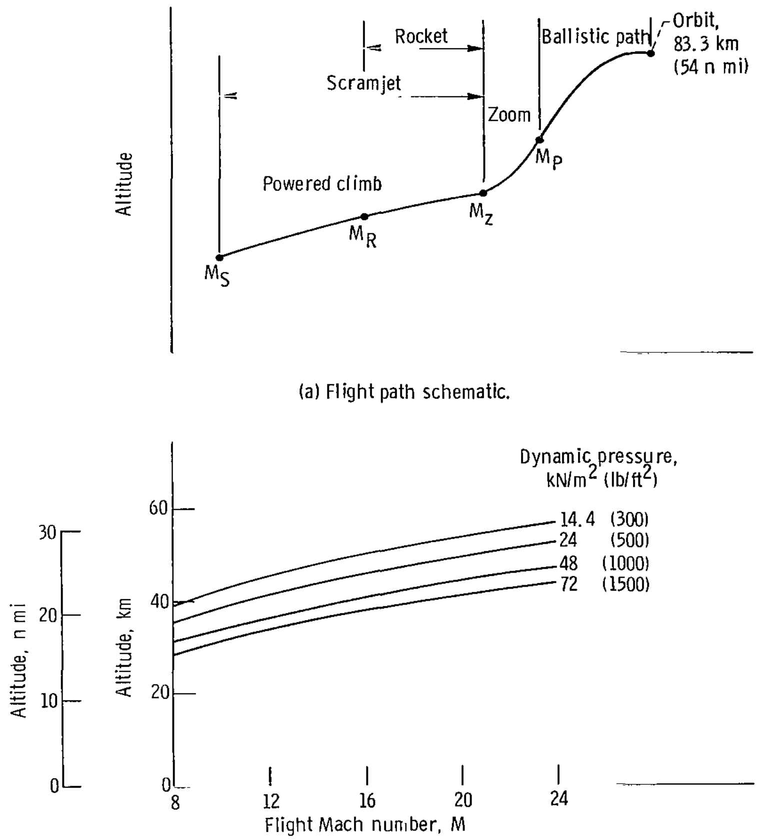

(a) Flight path schematic.

(b) Constant dynamic pressure flight paths.

Figure 2. - Second-stage flight paths.

due to launching from a latitude of 28° N at an azimuth of 55°. A schematic of the complete flight path and the constant q flight paths are shown in figure 2. The scramjet operates from the staging Mach number M_S to the zoom Mach number M_z. The rocket operates from the rocket-on Mach number M_R to the zoom Mach number and is also used for postorbital maneuvering as required. The zoom maneuver consists of a pullup in the atmosphere from the zoom Mach number to a pullup Mach number M_p on a ballistic path tangent at its peak to the 83.34-kilometer (54-n mi) perigee of the transfer ellipse. The zoom Mach number was determined by the method used in reference 10.

The equations of motion were integrated along the flight path up to zoom Mach number to obtain a time, range, velocity, acceleration, and weight history of the flight. Stage separation dynamics were not investigated.

Vehicle Aerodynamics, Skin Friction, and Heating

For calculation purposes, the vehicle was divided into seven flow regions. (See sketch (a) in appendix B.) The normal and axial force coefficients were determined for each region. Newtonian impact theory was used for compression flow fields such as the forebody cone. For expansion flow fields such as the top surface at positive angles of attack, Van Dyke's small disturbance theory was used. A normal force is also created on the vehicle rear cone surface by the expanding scramjet exhaust gas. The scramjet normal force coefficient was determined for each point of the flight path by integrating the pressure distributions on the rear cone surface and cowl which were approximated by one-dimensional flow analysis. The regional force coefficients plus the scramjet normal force coefficients were then summed resulting in overall vehicle normal and axial force coefficients. The bluntness drag coefficients for the wings, vertical stabilizer, and scramjet cowl were determined from Newtonian impact theory assuming leading edge diameters of 10.16 centimeters (1/3 ft). The average skin friction coefficient for a turbulent boundary layer was calculated for each flow region along the flight path accounting for variations in altitude, speed, and angle of attack. The internal friction drag of the scramjet surfaces was included in the scramjet engine performance.

The vehicle lift and drag coefficients were then determined from the relations:

$$\begin{aligned} C_L &= C_N \cos \alpha - C_A \sin \alpha \\ C_D &= C_N \sin \alpha + C_A \cos \alpha + C_F + C_{D_{BL}} \end{aligned} \tag{1}$$

A detailed analysis of the vehicle aerodynamics and skin friction is found in appendix B. Figure 3 shows lift and drag coefficients against angle of attack for the base-line vehicle. Figure 4 shows lift-drag ratios against Mach number and indicates the lift due to the centrifugal effect. It is seen that the centrifugal force contributes about 40 percent of the total or effective lift at Mach 15 and 100 percent at Mach 24. It is also seen that the nozzle or jet lift is a small part of the total lift. Curves of angle of attack and time against Mach number are shown in figure 5. The increase in centrifugal lift with Mach number reduces the aerodynamic component of total lift required for flight resulting in the decrease in angle of attack with Mach number shown in the figure.

Aerodynamic heating calculations were made to determine the thermal protection system weight of each vehicle. A time history of the average radiation equilibrium temperatures was calculated for each flow region of the vehicle. These calculations were accomplished in conjunction with the skin friction calculations. The equilibrium temperature history was then used in a one-dimensional transient heat conduction analysis to de-

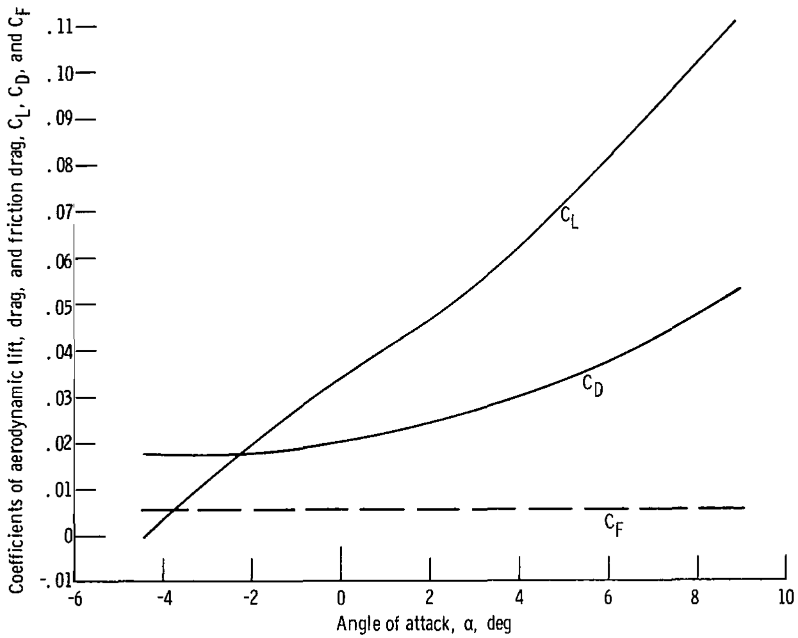

Figure 3. - Example of variation of lift and drag coefficients with angle of attack. Flight Mach number, 15; flight path dynamic pressure, 24 kilonewtons per square meter (500 lb/ft^2).

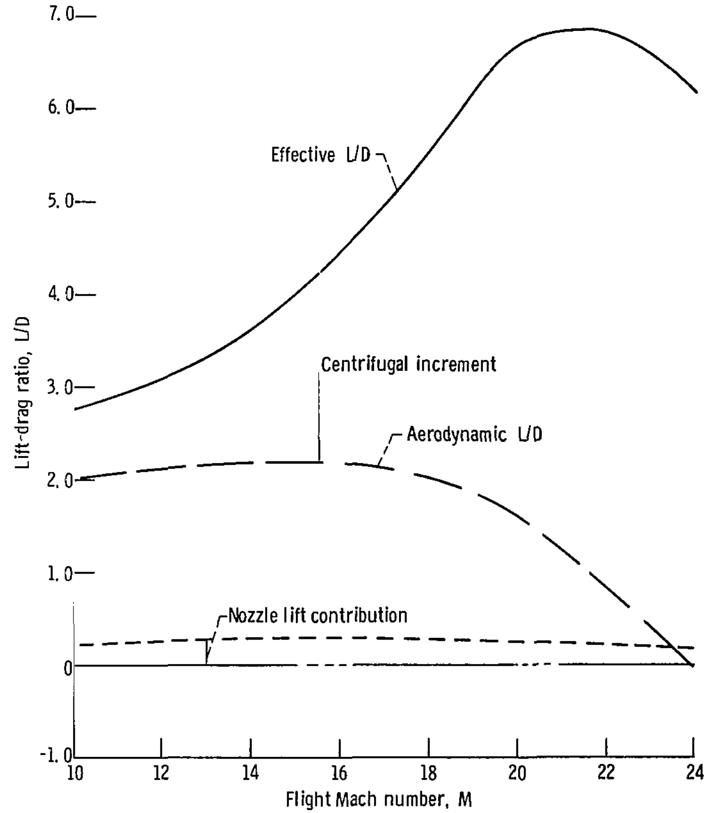

Figure 4. - Variation of lift-drag ratio with flight Mach number for the baseline configuration. Flight path dynamic pressure, 24 kilonewtons per square meter (500 lb/ft^2).

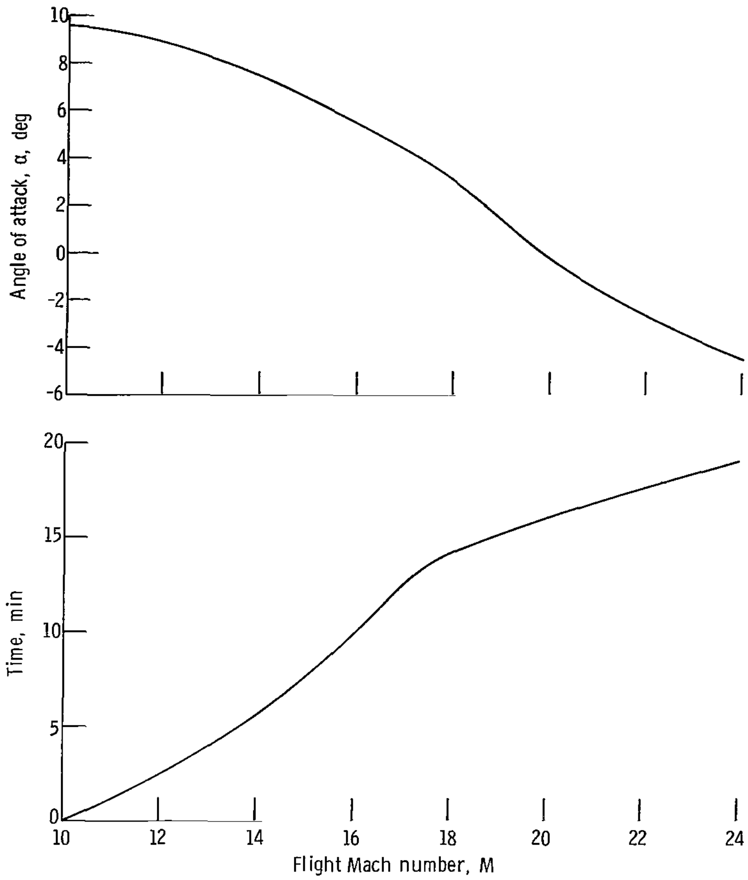

Figure 5. - Variation of angle of attack and time for baseline configuration. Flight path dynamic pressure, 24 kilonewtons per square meter (500 lb/ft^2).

termine the insulation requirements of each region of the vehicle. Additional details are given in appendix B.

Weight Analysis

Vehicle. - A cold primary structure was assumed with thermal protection of insulation and radiant heat shields. The primary structure weight estimates were based on lightweight metals such as aluminum. Nonintegral tanks with insulation such as polyurethane were assumed for the liquid hydrogen and oxygen. The insulation thickness was determined for a limiting backside temperature of 367 K (660° R) using the radiation equilibrium temperature histories and transient heat analysis mentioned in the previous section. The insulation weight was based on the properties of dyna-quartz with a density of 104.1 kilograms per cubic meter (6.5 lb/ft^3). A unit weight of 6.84 kilograms per square meter (1.4 lb/ft^2) (ref. 11) was used for the radiant heat shields assuming materials such as niobium or tantalum.

Engines. - The scramjet cowl primary structure was assumed to be of steel-type material compatible with 1000 K (1800° R) metal temperature. The primary structure weight was determined from hoop stress analysis using the highest internal pressure experienced along the flight path (appendix C) which generally was on the order of 4 to 5 atmospheres. Regenerative cooling panels on the inside surface and insulation and radiant heat shields on the exterior were assumed. Regenerative cooling panels were also assumed for the body surfaces exposed to the scramjet exhaust gas. The cooling panels were assumed to be materials such as Rene or Hastelloy. A unit weight of 11.2 kilograms per square meter (2.29 lb/ft^2) was used (ref. 12) based on a maximum metal temperature of 1000 K (1800° R).

The rocket engine weight including installation was estimated as 3 percent of the thrust.

The size of the four hydrogen-fueled turbofan engines was based on a thrust to vehicle reentry weight of 8.22 newtons per kilogram (0.38 lb/lb) and sea level thrust per unit air flow of 641 newtons per kilogram per second (261 lb/sec). The engine weight was estimated from

$$W_{TJ} = 4240\left(\frac{\dot{w}_{a_{TJ}}}{120.3}\right)^{1.2} \quad \text{(kg)}$$

or (3)

$$W_{TJ} = 9340\left(\frac{w_{a_{TJ}}}{265}\right)^{1.2} \quad \text{(lb)}$$

The results from this relation compare well with those presented in reference 13.

Further details of the weight analysis are given in appendix C. A unit weight breakdown for a typical vehicle is presented in figure 6. Including thermal protection, a typical unit body weight is 33.2 kilograms per square meter (6.8 lb/ft^2) of wetted surface area, and the unit wing weight is 66.2 kilograms per square meter (13.6 lb/ft^2) of wing planform area. The scramjet unit weight including regenerative cooling panels is 145.5 kilograms per square meter (29.8 lb/ft^2) of cowl surface area or 138.8 kilograms per square meter (28.5 lb/ft^2) or capture area. Body and wing unit weights for the rocket-powered shuttle second stage from reference 14 are 22.9 kilograms per square meter (4.69 lb/ft^2) and 41.7 kilograms per square meter (8.54 lb/ft^2), respectively. Table I shows the vehicle empty weight breakdown. The largest contributors to the empty weight are the basic body and thermal protection system, each comprising about 25 percent of the total empty weight. In comparison, the scramjet weight is about 15 percent.

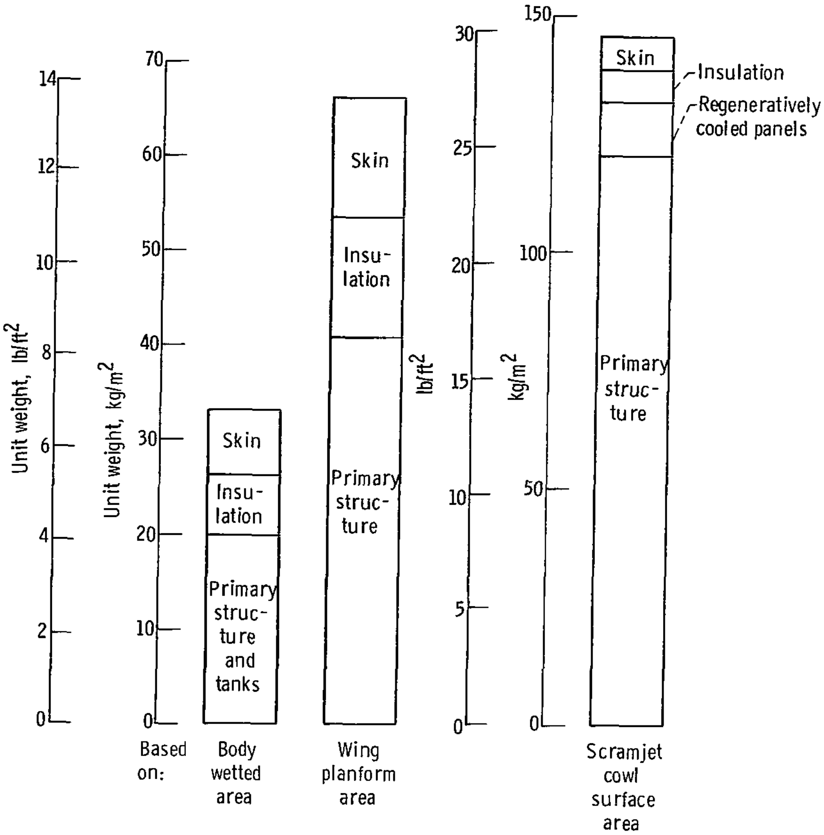

Figure 6. - Example of component unit weights. Stage weight, 227 000 kilograms (500 000 lb).

TABLE I. - EMPTY WEIGHT BREAKDOWN

Component	Weight, kg (lb)	Percent of total empty weight
Structure	64 620 (142 400)	87.70
Basic body	21 306 (47 000)	27.29
Thermal protection system	19 562 (43 120)	25.03
Fins	3 870 (8 535)	4.95
LH_2 and LOX tanks	4 831 (10 650)	6.18
Landing gear	3 632 (8 000)	4.65
Scramjet	11 419 (25 190)	14.62
Engines	8 030 (17 700)	10.28
Rocket	2 452 (5 400)	3.14
Turbofans	5 578 (12 290)	7.14
Equipment	5 448 (12 000)	6.97
Total	78 098 (172 200)	100.00

Scramjet. - The present engine configuration was adopted for simplicity in weight and aerodynamic analysis and was intended to provide first-order effects. The design of an actual engine would be much more integrated and compatible with vehicle flow fields. For example, contouring of the inlet compression and exhaust expansion surfaces may be necessary to meet the assigned performance levels. However, the scramjet performance used in this study is comparable to that expected from advanced engine designs. The engine configuration shown in figure 7 has a cylindrical cowl wrapped around the underside of the vehicle centerbody. The engine size or capture area was varied by the cowl central angle ψ shown in figure 7. The capture area is then defined by the area included in the angle ψ and the cowl radius r. The bottom of the vehicle forebody cone serves as the compression surface for the air entering the engine. The aft cone serves as the exhaust gas expansion surface. The axial location of the cowl leading edge relative to the vehicle body was fixed at the end of the forebody cone. Preliminary estimates of hydrogen-air mixing and reaction lengths indicated a 1.83-meter (6-ft) combustor length was adequate. The length of the vehicle centerbody, which serves as the inner wall of the constant area combustor was therefore fixed at 1.83 meters (6 ft). The cowl was extended beyond the end of the combustor by a length equal to 25 percent of the rear cone length to provide an outer expansion surface for the exhaust gas. Calculations indicated the best engine performance was obtained for a nozzle area ratio of about 30 for the range of flight Mach numbers considered in this study. A nozzle area ratio of 30 was therefore fixed for determining the scramjet engine performance. This also

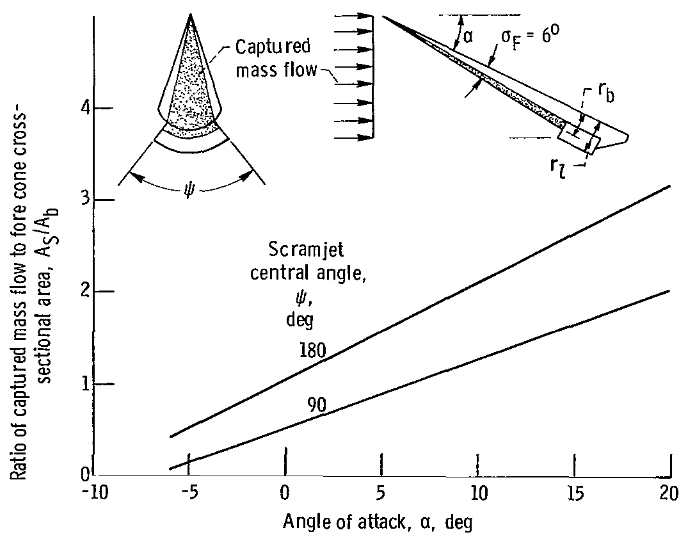

Figure 7. - Dependence of captured mass flow on angle of attack α and scramjet central angle ψ.

fixes the capture radius r_l in relation to the body radius r_b. Since the combustor and nozzle surfaces are assumed to be cooled with hydrogen fuel, a preliminary analysis was made of the required equivalence ratios since they influence scramjet performance, tankage volume, and vehicle size.

Although the internal flow conditions in the engine would vary with time, the analysis treats each point on the flight path as a steady-state condition. In order to determine the total heat absorbed by the hydrogen, the gas-side local heat transfer rates in the combustor and nozzle were calculated by the method of reference 15. The total heat transfer rate $\dot{Q}$ was then determined by integrating the local rates over the combustor and nozzle wall surfaces. The hydrogen was assumed to be a gas at 56 K (100° R) before entering the cooling system. A constant wall temperature of 1000 K (1800° R) was assumed although it was recognized that in real engines all parts of the engine are not the same temperature. The cooling equivalence ratio was determined from the following simplified expressions:

$$\dot{w}_f = \frac{\dot{Q}}{\eta_e \ \Delta H}$$

$$\varphi_c = \frac{\dot{w}_f/\dot{w}_a}{0.0292}$$

The η_e represents the fraction of the theoretical fuel enthalpy rise that may be realized in a real cooling system design. A value of 0.85 was used in this study. The cooling equivalence ratios for a typical vehicle are shown in figure 8 for flight Mach numbers

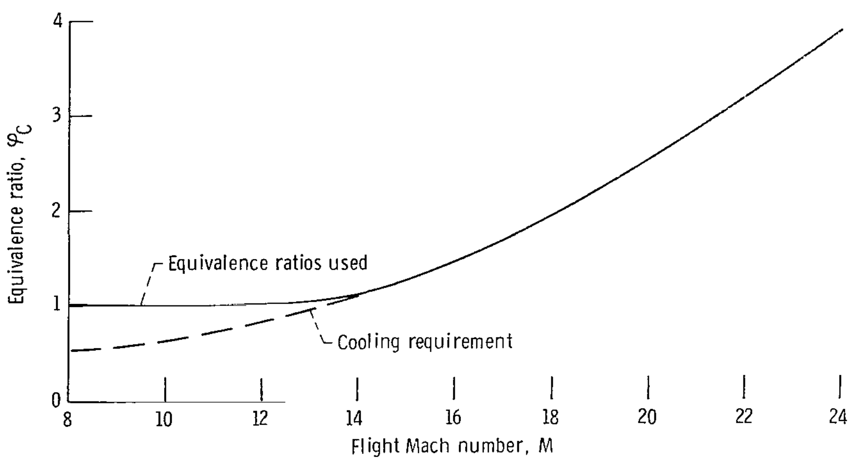

Figure 8. - Equivalence ratio schedule based on scramjet cooling requirements. Flight path dynamic pressure, 48 kilonewtons per square meter (1000 lb/ft^2).

from 8 to 24. Based on these preliminary estimates, stoichiometric fuel to air ratios appear adequate for engine cooling up to Mach numbers of about 14. However, equivalence ratios ranging from 1.25 at Mach 15 to 3.85 at Mach 24 would be required.

Rocket. - The hydrogen-oxygen rocket engine was assumed to have a chamber pressure of 21×10^6 newtons per square meter (438 lb/ft^2; 3000 $lb/in.^2$) and a nozzle area ratio of 120. The specific impulse based on an overall efficiency of $97\frac{1}{2}$ percent was determined from reference 16 to be 454 seconds for a mixture ratio of 8. A mixture ratio of 6 and specific impulse of 459 seconds were also used since these correspond to present shuttle orbiter engine performance, however, only minor changes in payload were calculated. The rocket size was varied to maximize payload and was determined by specifying the propellant weight flow rate $\dot{w}_r$. The nozzle exit area was calculated from the weight flow rate and flow rate per unit exit area determined from reference 16. To provide space for housing the engine in the rear of the vehicle, the length of the rocket engine compartment was assumed to be twice the diameter of the nozzle exit.

Scramjet engine performance. - Since the vehicle forebody cone acts as an inlet compressive surface, the shock and friction losses of the air entering the engine are accounted for in the forebody pressure and friction drags. The cowl bluntness and exterior friction drags were added to the vehicle drag. The nozzle aft cone friction drag was determined assuming a turbulent boundary layer using the method of reference 15. The friction loss was then accounted for in the engine performance by conversion to nozzle efficiency factors shown in figure 9.

Scramjet nozzle dissociation losses are dependent on many variables, that is, engine size, nozzle shape, inlet performance, and fuel-air ratio. It was considered beyond the scope of this study to investigate these losses for the simplified engine configuration adopted in this study. However, reference 17 indicates scramjet dissociation losses are small for stoichiometric fuel-air ratios and reference 18 shows that they decrease with increasing equivalence ratios. Since equivalence ratios are considerably greater than

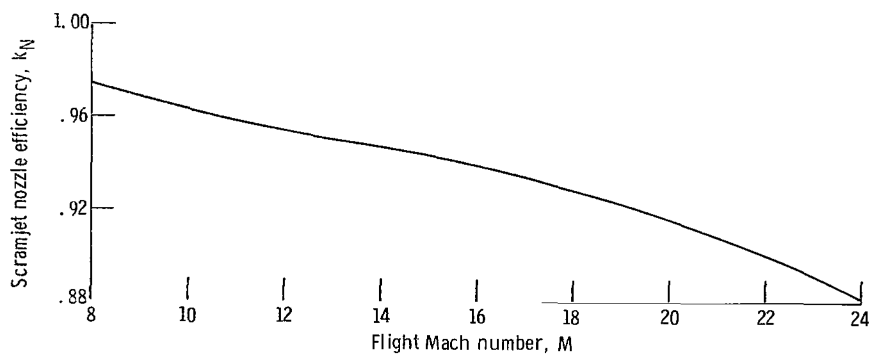

Figure 9. - Scramjet nozzle efficiency factors. $K_N = \left(V_e^2 - V_{CB}^2\right)/\left(V_{e_{ID}}^2 - V_{CB}^2\right)$ where V_{CB} is combustor exit velocity, V_e is nozzle exit velocity, and $V_{e_{ID}}$ is ideal nozzle exit velocity.

unity for a large part of the flight path in this study, the scramjet specific impulse was calculated using the equivalence ratio schedule of figure 8 assuming chemical equilibrium, a nozzle area ratio of 30, and a combustion efficiency of 90 percent.

The engine performance estimate accounts for variations in flight path dynamic pressure and inlet compression ratio variations due to vehicle angle of attack for the range of flight Mach numbers considered in this study. The relative size of scramjet to rocket was determined by specifying the augmentation ratio $\dot{w}_a/\dot{w}_r$ at the rocket-on Mach number. The effective specific impulse is the combined thrust of scramjet and rocket $(F_{sc} + R_{ROC})$ divided by the sum of the scramjet hydrogen flow rate and rocket propellant flow rate $(\dot{w}_f + \dot{w}_r)$. Figure 10(a) shows the effective specific impulse for a typical case for a rocket-on Mach number of 18. The thrust to drag ratios for the scramjet, rocket, and combination of both engines are presented in figure 10(b). After the rocket is fired $(M_R = 18)$, the effective impulse is much lower than the scramjet impulse; however, the thrust to drag ratio is appreciably increased and results in better acceleration, smaller scramjet engine sizes, and weight savings. This effect is discussed further in the RESULTS AND DISCUSSION section. The augmentation ratio $\dot{w}_a/\dot{w}_r$ for this example varied from 5.2 at $M_R = 18$ to 2.1 at $M = 24$ since the airflow rate $\dot{w}_a$ decreases while the rocket propellant flow remains constant.

Figure 11(a) shows the scramjet specific impulse penalty resulting from the high equivalence ratios required for cooling. The performance decrement when compared to the stoichiometric ($\varphi = 1$) impulse is about 30 percent at Mach numbers above 18. Figure 11(b) compares the thrust coefficients for the two equivalence ratio schedules $\varphi > 1$ and $\varphi = 1$ and the vehicle drag coefficients. It is seen that an appreciable thrust minus drag margin can be maintained with fuel-rich operation but that for the stoichiometric schedule, the thrust and drag become equal at Mach 22. Since the scramjet is an integral part of the vehicle increasing the engine size results in a larger vehicle with added drag and weight penalties. Thus, scramjet-only propulsion with stoichiometric fuel-air ratios does not appear feasible for powering a second-stage vehicle to orbital velocities. This result was also indicated in reference 10. The significance of these two scramjet equivalence ratio schedules on vehicle payload is discussed in the RESULTS AND DISCUSSION section.

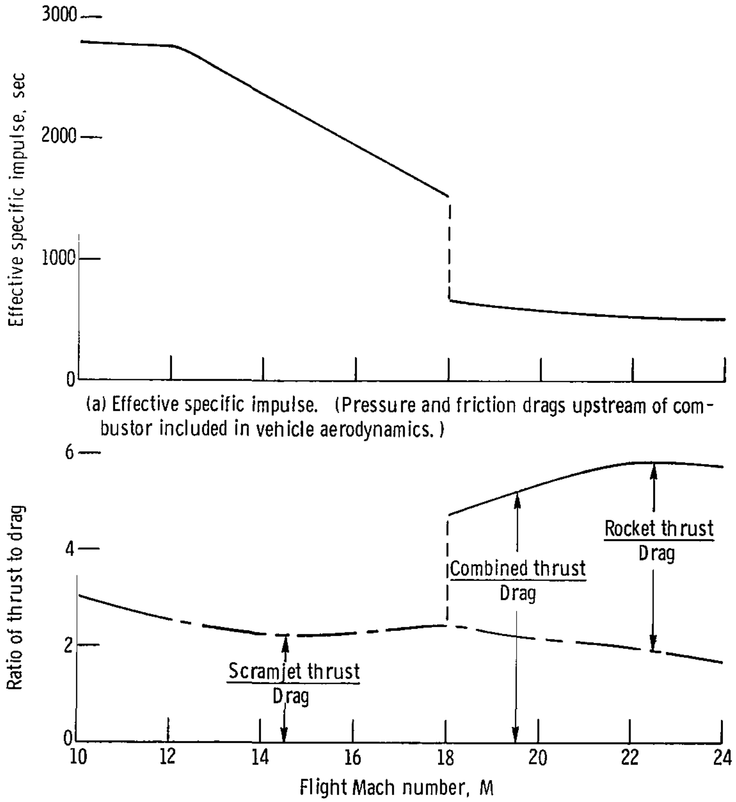

(a) Effective specific impulse. (Pressure and friction drags upstream of combustor included in vehicle aerodynamics.)

(b) Thrust to drag ratios.

Figure 10. - Effective specific impulse and thrust to drag ratios. Staging Mach number, 10; rocket-on Mach number, 18; flight path dynamic pressure, 24 kilonewtons per square meter (500 lb/ft^2); stage weight, 227 000 kilograms (500 000 lb).

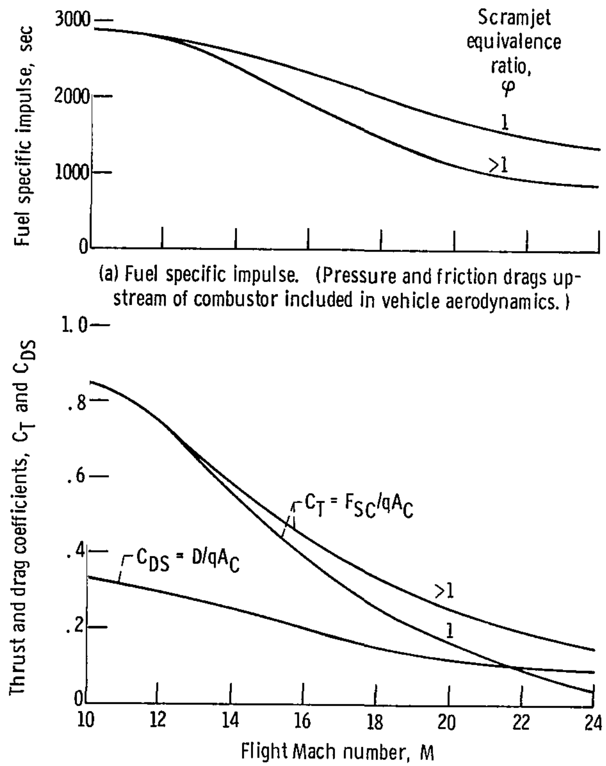

(a) Fuel specific impulse. (Pressure and friction drags upstream of combustor included in vehicle aerodynamics.)

(b) Thrust and drag coefficients.

Figure 11. - Effect of scramjet equivalence ratio on fuel specific impulse and thrust coefficient. Staging Mach number, 10; flight path dynamic pressure, 24 kilonewtons per square meter (500 lb/ft^2); stage weight, 227 000 kilograms (500 000 lb).

RESULTS AND DISCUSSION

The results of this study are presented in terms of payload delivered to 500-kilometer (270-n mi) circular orbit by a second-stage vehicle. The vehicle and engine parametric results are given for a stage weight of 227 000 kilograms (500 000 lb). The sensitivity of payload to scramjet performance, cooling requirements and jet lift, and vehicle structure and insulation weights, volumetric efficiency and friction drag are also shown.

Vehicle Configuration

Fore and aft cone angles. - Figure 12 shows the effect of vehicle forebody cone angle and aft cone angle on the percent payload. The best payloads result from small forebody

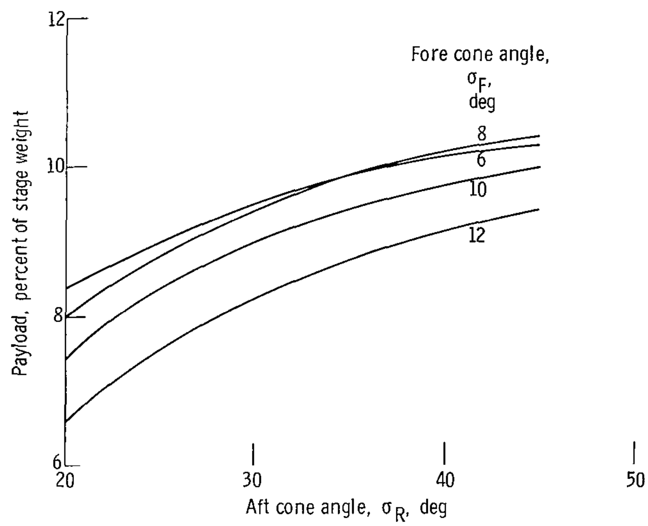

Figure 12. - Effect of vehicle fore and aft cone angles on payload. Staging Mach number, 10; rocket-on Mach number, 18; scramjet central angle, 180°; flight path dynamic pressure, 24 kilonewtons per square meter (500 lb/ft²); stage weight, 227 000 kilograms (500 000 lb).

cone angles of 6° to 8°. At the larger cone angles of 10° or 12°, the higher forebody pressure drag requires larger scramjet engines resulting in increased fuel and engine weights. It is also seen from figure 12 that short aft bodies with large cone angles of 40° to 45° result in best payload. Although the scramjet nozzle lift is doubled by reducing the rear cone angle from 45° to 20°, it comprises only a small part of the total lift (fig. 4). The increase in planform area at the small aft cone angles causes higher friction drag and weight resulting in a payload penalty.

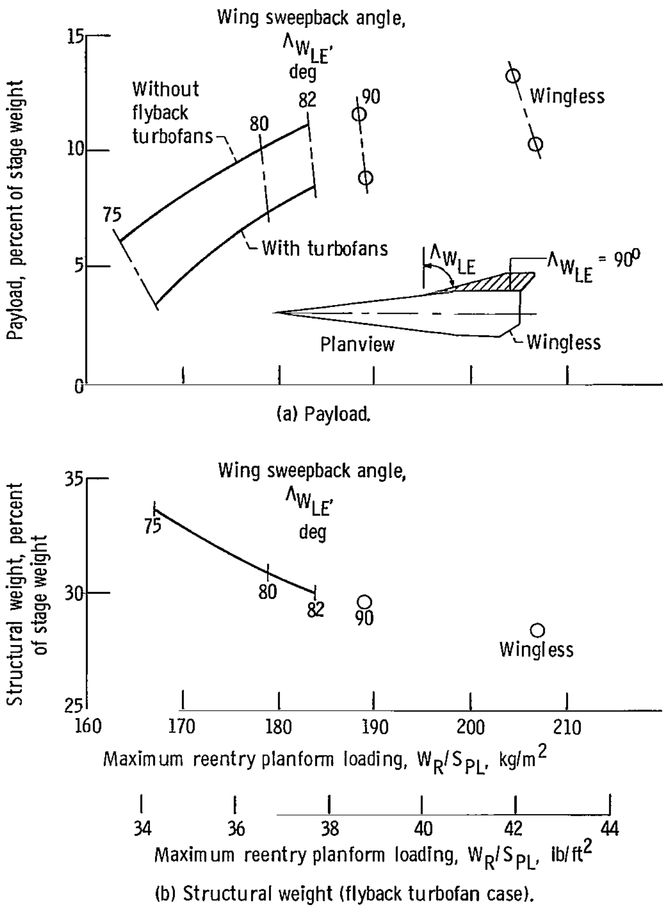

Figure 13. - Effect of wings and flyback turbofan engine weight on payload and structural weight. Staging Mach number, 10; rocket-on Mach number, 18; scramjet central angle, 180°; fore cone angle, 8°; aft cone angle, 45°; flightpath dynamic pressure, 24 kilonewtons per square meter (500 lb/ft^2) stage weight; 227 000 kilograms (500 000 lb).

Wings and flyback turbofans. - Figure 13(a) shows the variation of payload with planform loading and wing sweepback angle and also shows the effect of eliminating the flyback turbofan engines. The sweepback angle of 90° indicates that the wing projects from the aft section of the vehicle as depicted in the sketch labeled Planview shown in the figure. Adding wing area in order to decrease the planform loading, W_R/S_{PL} at the landing condition results in a drastic decrease in payload as shown in figure 13(a). As seen in figure 13(b), this is primarily the result of increased structural weight due to the added wing panels. As analyzed in this study, the lift-drag ratio for the forebody cone is slightly better than that for the wing at moderate angles of attack. Hence, the overall lift-drag ratio is not improved during ascent and the added wing weight and drag is a complete penalty.

In addition the aerodynamic lift becomes less significant as speed increases (fig. 4). Factors such as heating during reentry, cross range, and stability and control during the landing phase of a vehicle with no wings were not evaluated. Recent opinions observed in reference 19 indicate that the lifting body can be adequately controlled during approach and landing. In fact, the need for flyback or go-around turbofans is also dismissed in the same reference. The results of eliminating the flyback turbofans and their fuel are also shown in figure 13(a). An increase in payload of $2\frac{1}{2}$ to 3 percent of the staging weight is realized by eliminating the turbofan engines.

Engine Parameters

Scramjet engine sizing. - Figure 14 shows that the best payload is obtained when the cowl central angle is 180^{O}. For smaller scramjets ($\psi < 180^{\mathrm{O}}$) larger rockets (decreasing $\dot{w}_a/\dot{w}_r$) are needed earlier in the flight to provide the required thrust. This is shown by the indicated rocket sizes and rocket-on Mach numbers in table II. The lower effective specific impulse of the smaller scramjets and the longer rocket operation time increase propellant consumption, which offsets the lower scramjet engine weight and decreases payload.

Rocket-on Mach number and augmentation ratio. - Figure 15 shows that the payload is optimized at rocket-on Mach numbers of about 18. This is due to the tradeoff between propellant and structure weights. The bar chart of figure 16 shows this more clearly. The structural weight in the figure includes the thermal protection system. The higher thrust obtained by operating the rocket earlier in the flight decreases the total flight time and hydrogen consumption resulting in lighter structural weight. But the increase in LOX weight offsets the reduction in LH_2 and structural weights resulting in reduced payload. Delaying rocket operation beyond Mach 18 results in excessive LH_2 and structural weights and reduced payload.

The effect of augmentation ratio seen in figure 15 shows that small rocket sizes ($\dot{w}_a/\dot{w}_r$ = 10 to 15) result in higher payloads at low rocket-on Mach numbers, whereas, at high rocket-on Mach numbers, larger rockets result in the best payloads. Since the rocket operates for a much longer time period at low rocket-on Mach numbers, larger rockets lead to excessive propellant weight and payload penalties.

Also shown in figures 15 and 16 are the payload fractions and weight components for scramjet-only and rocket-only propulsion. The payload of the scramjet-only vehicle is 33 percent lower than the best augmented scramjet vehicle because elimination of the rocket thrust requires larger scramjet engines resulting in higher fuel and structural weights. The high propellant weight of the rocket-only vehicle results in a 41 percent lower payload when compared with the augmented scramjet vehicle. The aerodynamic

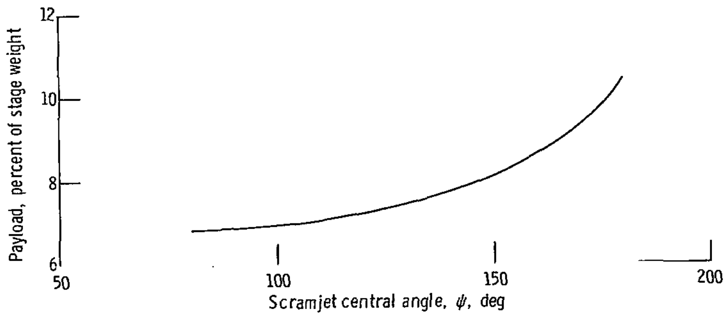

Figure 14. - Effect of scramjet engine size on payload. Staging Mach number, 10; rocket-on Mach number, 18; fore cone angle, 8°; aft cone angle, 45°; flight path dynamic pressure, 24 kilonewtons per square meter (500 lb/ft^2); stage weight, 227 000 kilograms (500 000 lb).

TABLE II. - AUGMENTATION RATIOS

AND ROCKET-ON MACH NUMBERS

THAT MAXIMIZE PAYLOAD

Scramjet central angle, ψ, deg	Augmentation ratio, $\dot{w}_a/\dot{w}_r$	Rocket-on Mach number, M_R
80	1.6	10
120	3.7	18
120	5.2	18

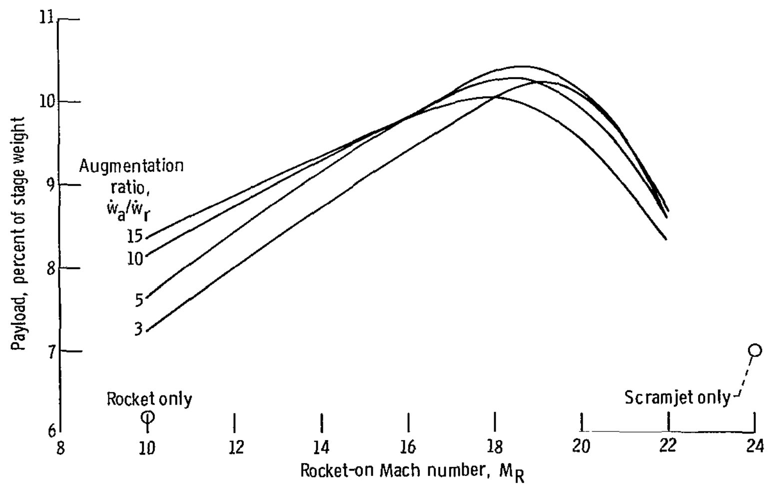

Figure 15. - Effect of rocket-on Mach number and augmentation ratio on payload. Staging Mach number, 10; scramjet central angle, 180°; fore cone angle, 8°; aft cone angle, 45°; flight path dynamic pressure, 24 kilonewtons per square meter (500 lb/ft^2); stage weight, 227 000 kilograms (500 000 lb).

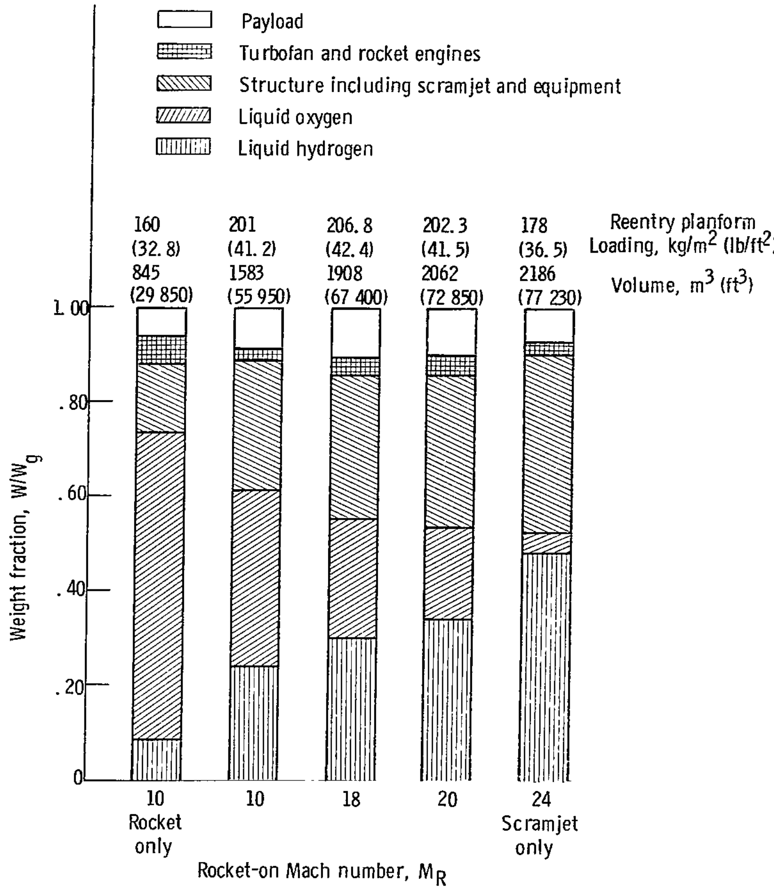

Figure 16. - Variation of weight fractions with rocket-on Mach number. Staging Mach number, 10; scramjet central angle, 180°; fore cone angle, 8°; aft cone angle, 45°; flight path dynamic pressure, 24 kilonewtons per square meter (500 lb/ft^2); stage weight, 227 000 kilograms (500 000 lb).

drag of the lifting flight path probably penalizes the rocket vehicle performance in comparison with a typical nonlifting rocket trajectory. The intent here, however, is to arrive at the best combination of scramjet and rocket engine sizes to obtain the best payload for the specific flight path. Table III shows a comparison of the augmented scramjet, scramjet-only, and rocket-only vehicles.

Baseline vehicle configuration. - The characteristics of the vehicle configuration used in the remaining parametric and sensitivity studies are given in table IV. Unless specified otherwise, a constant dynamic pressure flight path of 24 kilonewtons per square meter (500 lb/ft^2) and the equivalence ratio schedule of figure 8 were used.

TABLE III. - COMPARISON OF VEHICLES

	Augmented scramjet	Scramjet only	Rocket only
Vehicle weights			
Stage weight, kg (lb)	227 000 (500 000)	227 000 (500 000)	227 000 (500 000)
Empty weight, kg (lb)	78 000 (172 000)	89 500 (197 300)	45 400 (100 100)
Payload, kg (lb)	23 600 (52 080)	16 200 (35 700)	14 400 (31 750)
Vehicle dimensions			
Lemgth, m (ft)	62.5 (205)	70.0 (230)	45.8 (150)
Diameter, m (ft)	15.2 (49.9)	17.0 (55.8)	11.2 (36.75)
Planform area, m^2 (ft^2)	495 (5330)	603 (6490)	373 (4020)
Volume, m^3 (ft^3)	1098 (2053)	2580 (2776)	800 (8610)
Propulsion			
Scramjet thrust, kN (lb)	1500 (337 500)	1825 (410 600)	------- -------
Rocket thrust, kN (lb)	800 (180 000)	------- -------	3200 (720 000)
Augmentation ratio	5.2 (5.2)		
Staging Mach number	10 (10)	10 (10)	10 (10)
Rocket-on Mach number	18 (18)	------- -------	10 (10)
Acceleration time, min	19.1 (19.1)	31.1 (31.1)	3.7 (3.7)
Acceleration range, km (n mi)	6060 (3270)	12 000 (6475)	1100 (5940)
Maximum acceleration, g	1 (1)	1 (1)	4.5 (4.5)

TABLE IV. - BASELINE VEHICLE CHARACTERISTICS

Forward cone semi-angle, σ_F, deg	8
Rear cone semi-angle, σ_R, deg	45
Scramjet central angle, ψ, deg	180
Wing leading edge sweepback angle, $\Lambda_{W_{LE}}$	Wingless
Vertical stabilizer leading edge sweepback angle, $\Lambda_{S_{LE}}$, deg	60
Volume to planform parameter, $V_b^{2/3}/S_{PL}$	0.311
Vehicle span to length ratio, b/l	0.246
Vehicle surface area to volume parameter, $S_{WF}/V_b^{2/3}$	8.53
Vehicle cross-sectional area to volume parameter, $A_b/V_b^{2/3}$	0.573

Stage Weight and Flight Path

The increase in payload fraction with increasing stage weight is shown in figure 17. This is mainly the result of the volume-surface effects of lower structural weight fractions for larger vehicles.

In addition, the figure shows that the best constant dynamic pressure flight path q ranges from 24 to 48 kilonewtons per square meter (500 to 1000 lb/ft^2). This result is strongly related to the effect of dynamic pressure on scramjet thrust and the tradeoff between thermal protection system and propellant weights. Since the engine airflow per unit capture area decreases with increasing altitude, engine thrust levels decrease with

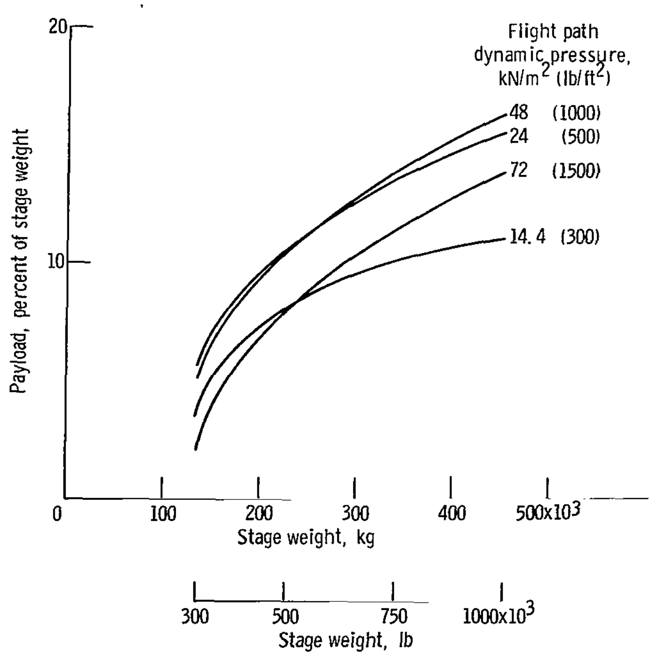

Figure 17. - Effect of stage weight and flight path on payload. Staging Mach number, 10; rocket-on Mach number, 18.

decreasing dynamic pressure flight paths. Although the thermal protection requirements would be expected to become less stringent by decreasing flight path q's, the lower scramjet thrust levels result in longer flight times which increase both thermal protection weight and propellant weight. For example, for a stage weight of 227 000 kilograms (500 000 lb), lowering the flight path q from 24 to 14.4 kilonewtons per square meter (500 to 300 lb/ft^2) decreases the scramjet thrust to vehicle weight ratio from 0.7 to 0.4 and increases flight time from 19 to 31 minutes. The resulting increase in thermal protection and propellant weights are 1 percent and $2\frac{1}{2}$ percent of stage weight, respectively, and the payload decreases by 3 percent. Larger rockets reduce time and insulation weight but this is offset by excessive rocket propellant consumption. Also, since the scramjet is an integral part of the vehicle, larger scramjets oversize the vehicle beyond the volume requirements leading to heavier structural weights and payload penalties. At a constant q flight path of 72 kilonewtons per square meter (1500 lb/ft^2), scramjet thrust is much higher but vehicle drag is also increased such that scramjet engine sizes are essentially as large as those for flight path q's of 24 or 48 kilonewtons per square meter (500 or 1000 lb/ft^2) resulting in reduced flight time and insulation weight but higher propellant weight. Between flight path q's of 24 to 48 kilonewtons per square meter (500 to 1000 lb/ft^2), the tradeoff between propellant weight and insulation weight is about even resulting in payloads of 10 percent of stage weight.

Another influencing factor is that the centrifugal force contributes such a large part of the lift that the vehicle effective lift (centrifugal plus aerodynamic) is relatively unaffected by flight path. However, the lower drag resulting from lower dynamic pressures results in an increase of lift-drag ratio with decreasing dynamic pressure flight paths.

Staging Mach Number

Typically, second-stage payload fraction improves with increasing staging Mach numbers. This is illustrated in figure 18. However, choosing the best staging Mach number involves consideration of the first-stage characteristics also. Although an in depth investigation of this type is beyond the scope of this study, trajectory calculations were made to obtain estimates of the propellant mass fractions of a vertical takeoff rocket-powered first stage for staging Mach numbers from 8 to 12 for a horizontal burnout at a dynamic pressure of 24 kilonewtons per square meter (500 lb/ft^2). This value of dynamic pressure is near the optimum for the second-stage acceleration (fig. 17). Ten percent of

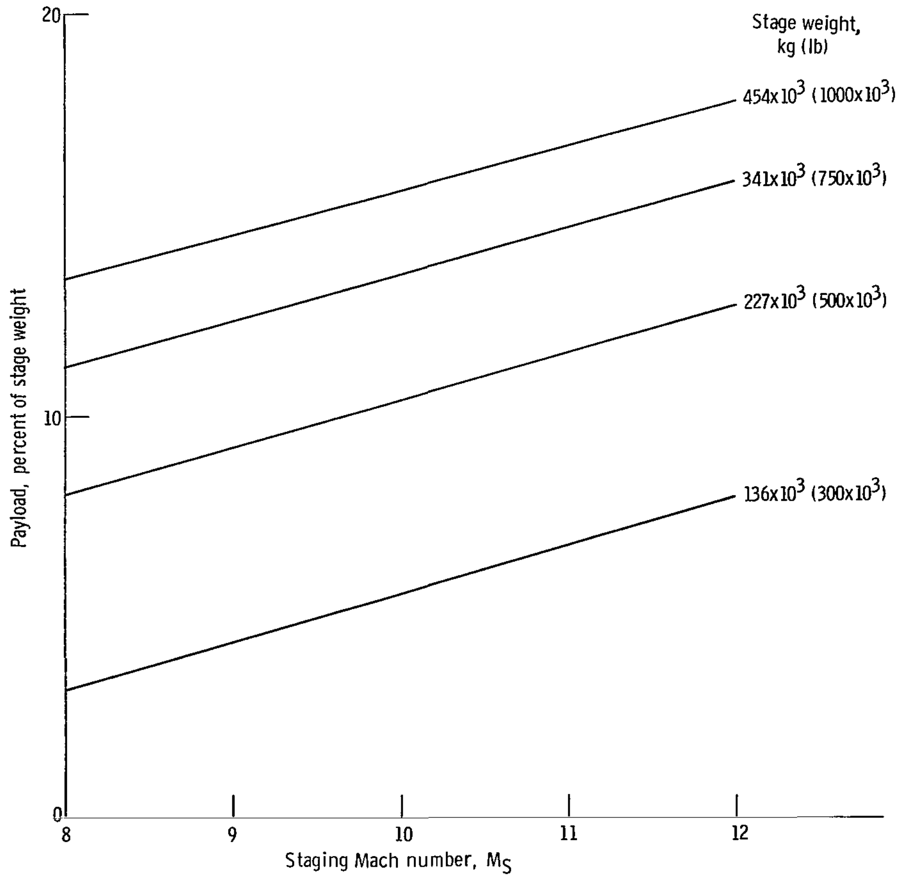

Figure 18. - Effect of staging Mach number on payload. Rocket-on Mach number 18; flight path dynamic pressure, 24 kilonewtons per square meter (500 lb/ft^2).

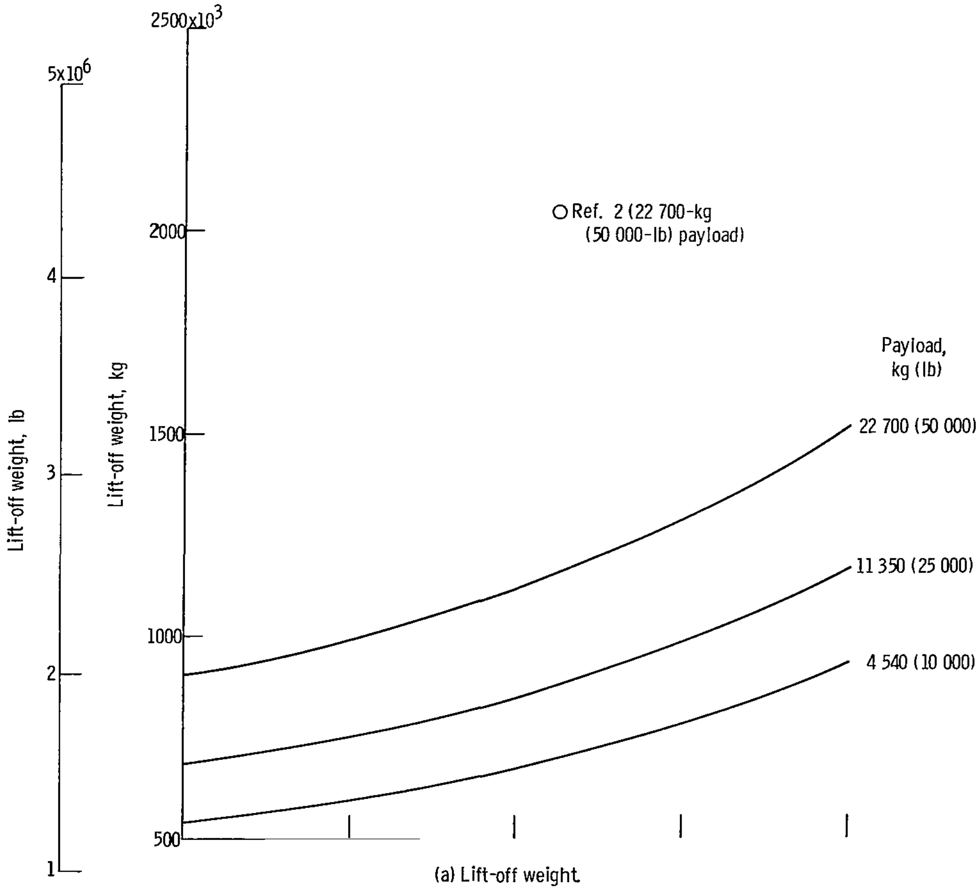

(a) Lift-off weight.

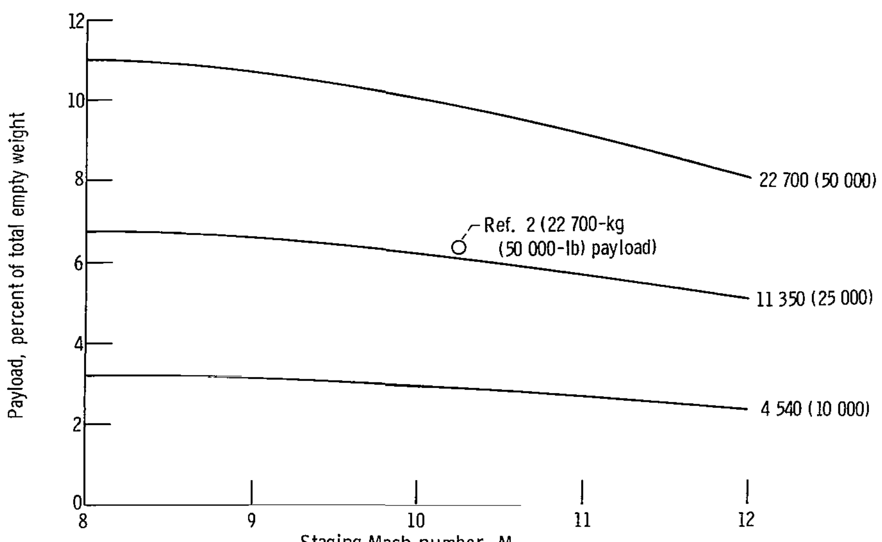

(b) Payload to total empty weight fraction.

Figure 19. - Effect of staging Mach number on lift-off weight and payload to total empty weight ratio for rocket first stage, augmented scramjet second stage. Rocket-on Mach number, 18; second-stage flight path dynamic pressure, 24 kilonewtons per square meter (500 lb/ft^2).

the first-stage entry weight was assumed for first-stage reserves and flyback fuel. Hardware weight estimates were obtained from data in reference 14 for shuttle vehicles. These considerations of the first stage are included in figure 19 which shows the effect of staging Mach number in terms of total lift-off weight and payload to total empty weight fraction. The optimum staging Mach number is about 8. For comparison, the weight estimated for the all-rocket-powered shuttle vehicle of reference 2 are shown. For the same payload, the lowest lift-off weight of the vehicle considered in this study is 56 percent lower than that of the all-rocket vehicle and the lowest empty weight is about 42 percent lower. However, stage separation dynamic problems would be more severe at this dynamic pressure level. In addition, first-stage hardware weight penalties may be incurred because of the different trajectory required to stage at a dynamic pressure of 24 kilonewtons per square meter (500 lb/ft^2). Although maximum q's of about 24 kilonewtons per square meter (500 lb/ft^2) are encountered on a typical first-stage rocket vehicle trajectory, staging at this q level requires the vehicle to experience these dynamic pressure loads and thermal environment for a longer period of time requiring heavier structure and thermal protection weights. A calculation of this penalty was not made; however, figure 20 shows the sensitivity of lift-off weight and payload to empty weight fraction to increases in first-stage empty weight for a staging Mach number of 8. A 25 percent increase in first-stage empty weight would still result in decreases in lift-off and empty weights of 49 and 29 percent, respectively, for a payload of 22 700 kilograms (500 000 lb) compared with the all-rocket-powered vehicle of reference 2. For a 60 percent increase, the lift-off weight is still 37 percent lower but the empty weight is about the same.

Sensitivity Studies

Scramjet equivalence ratio. - Figure 21 shows that the higher thrust levels attainable with fuel-rich scramjet operation lead to higher payload fractions than stoichiometric operation. At flight Mach numbers above 19, where the stoichiometric scramjet thrust is not much higher than vehicle drag (fig. 11(b)), rocket augmentation is required to accelerate to the zoom velocity in order to reduce flight time and excessive fuel consumption and structural and insulation weights. This is seen by the large drop in payload fraction for the stoichiometric scramjet when rocket operation is delayed beyond flight Mach numbers of 19. The fuel-rich scramjet supplies enough thrust so that rocket augmentation is not as critical even though a payload penalty is incurred by all-scramjet-propulsion in comparison to augmenting the scramjet. Table V supports some of the aforementioned observations for the stoichiometric and fuel-rich scramjet operation for a rocket-on Mach number of 21.

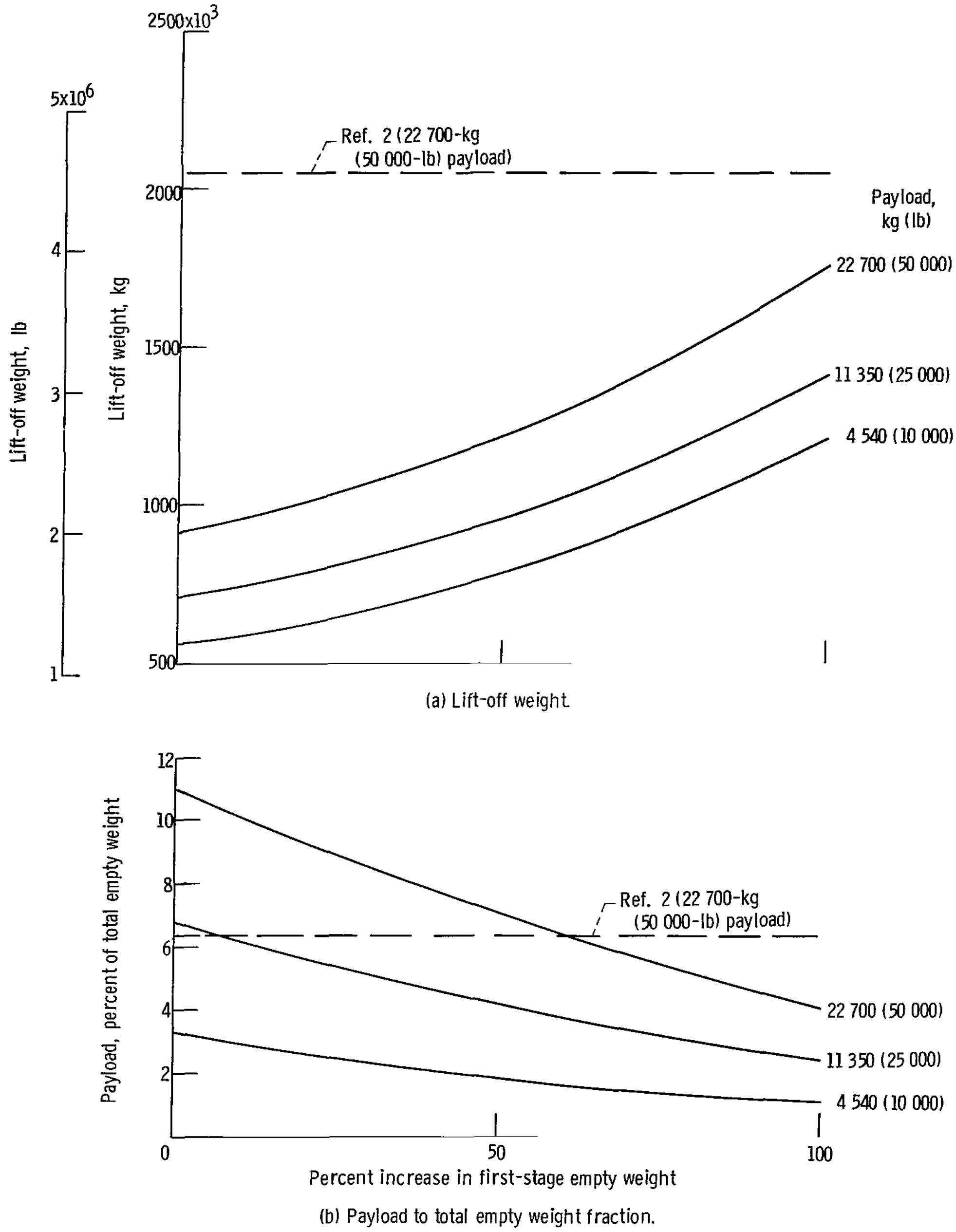

Figure 20. - Effect of first-stage empty weight on lift-off weight and payload to total empty weight ratio for rocket first stage, augmented scramjet second stage. Staging Mach number, 8; rocket-on Mach number, 18; second-stage flight path dynamic pressure, 24 kilonewtons per square meter (500 lb/ft^2).

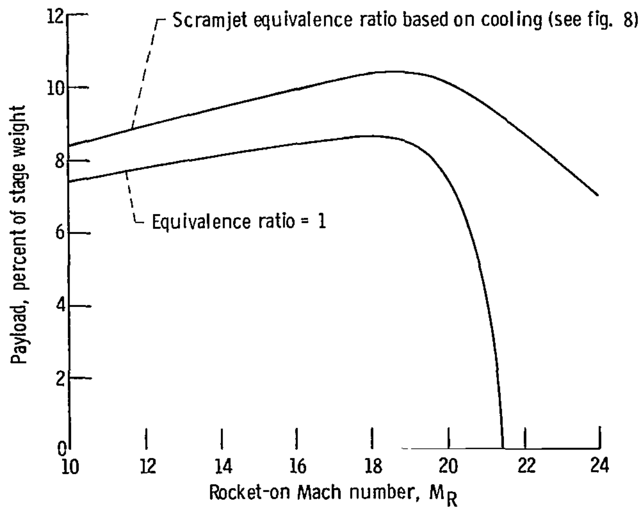

Figure 21. - Effect of scramjet equivalence ratio on vehicle payload. Staging Mach number, 10; flight path dynamic pressure, 24 kilonewtons per square meter (500 lb/ft^2); stage weight, 227 000 kilograms (500 000 lb).

TABLE V. - COMPARISON OF FUEL RICH AND STOICHIOMETRIC

	Fuel rich	Stoichiometric
Payload, kg (lb)	21 600 (47 650)	10 000 (22 040)
LH_2, kg (lb)	84 600 (186 600)	92 000 (202 900)
LOX, kg (lb)	35 200 (77 650)	39 300 (86 650)
Structure, kg (lb)	76 500 (168 700)	77 700 (171 300)
Insulation, kg (lb)	22 300 (49 200)	23 900 (52 700)
Augmentation ratio	5.55 (5.55)	5.5 (5.5)
Scramjet thrust at Mach 21, kN (lb)	510 (114 600)	286 (64 300)
Volume, m^3 (ft^3)	2190 (77 300)	2150 (75 900)
Flight time, min	23.2 (23.2)	48.0 (48.0)

Scramjet engine performance. - Since the hydrogen used by the scramjet comprises about 25 percent of the stage weight, engine performance would be expected to significantly affect payload. The sensitivity of payload to engine performance was determined by varying the calculated scramjet specific impulse by a fixed percentage over the flight path. The strong effect the engine performance exerts on vehicle payload is shown in figure 22. A 10 percent increase in specific impulse would raise the payload by 30 percent. A 12 percent decrease would lower the payload by 40 percent which would result in payload comparable to that of the rocket-powered second stage.

Vehicle aerodynamics. - The sensitivity of payload to vehicle aerodynamics was studied by varying the calculated lift and drag by a fixed percent over the flight path. Figure 23 shows that the payload is not significantly affected by a wide variation in aerodynamic lift since the centrifugal effects are so large (see the section Vehicle Aerodynamics, Skin Friction, and Heating). The drag, however, has a much greater effect since payload changes by about 14 percent for a 10 percent variation in drag.

The sensitivity of payload to scramjet lift was also investigated by setting the scramjet lift equal to zero. As might be expected, however, it had a negligible effect on payload, since it comprised such a small part of the total lift (fig. 4).

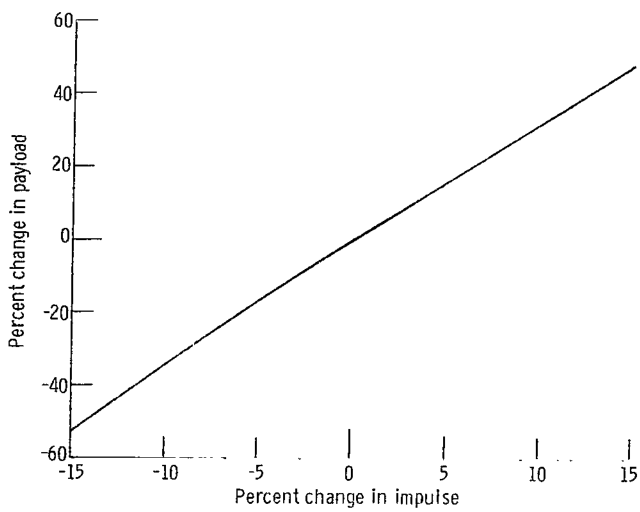

Figure 22. - Effect of scramjet fuel specific impulse on payload. Staging Mach number, 10; rocket-on Mach number, 18; flight path dynamic pressure, 24 kilonewtons per square meter (500 lb/ft^2); stage weight, 227 000 kilograms (500 000 lb); base payload, 23 500 kilograms (51 800 lb).

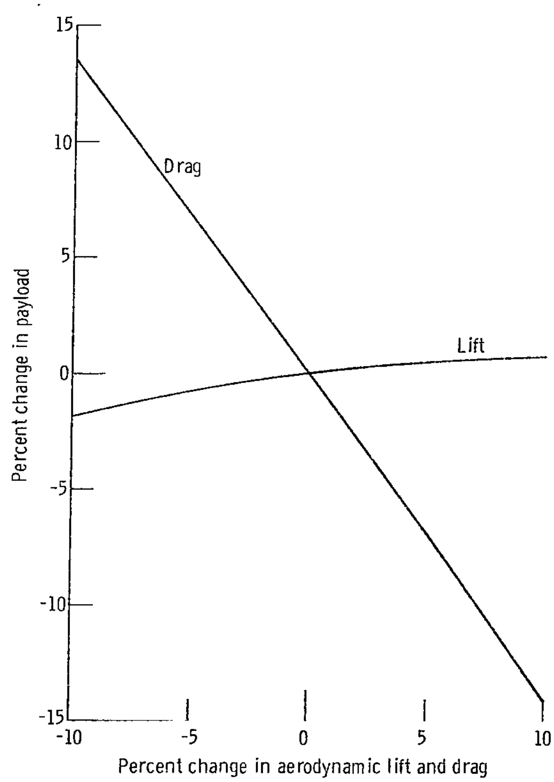

Figure 23. - Effect of vehicle aerodynamics on payload. Staging Mach number, 10; rocket-on Mach number, 18; flight path dynamic pressure, 24 kilonewtons per square meter (500 lb/ft^2); stage weight, 227 000 kilograms (500 000 lb); base payload, 23 500 kilograms (51 800 lb).

Vehicle volumetric efficiency. - Figure 24 shows that vehicle volumetric efficiency has a significant effect on payload. This can be expected since it directly affects vehicle size and structural weight. The volumetric efficiency assumed for this study was 75 percent. It is seen in the figure that a change in volumetric efficiency of 10 percent results in about a 10 percent change in payload.

Structural and insulation weight. - The sensitivity of vehicle payload to vehicle structural and insulation weights is shown in figure 25. A 20 percent increase in insulation weight and structural weight (less insulation) decreases the payload by 12.5 percent and 21 percent, respectively. Reference 20 indicates substantial promise for replacing metallic shingles with reusable external ceramic insulation. Advantages would include a 25 percent reduction in the thermal protection system weight compared with the system used herein, a high maximum surface temperature capability and other operating benefits. Such a reduction in thermal protection weight would result in a 15.8 percent increase in payload as seen in figure 25.

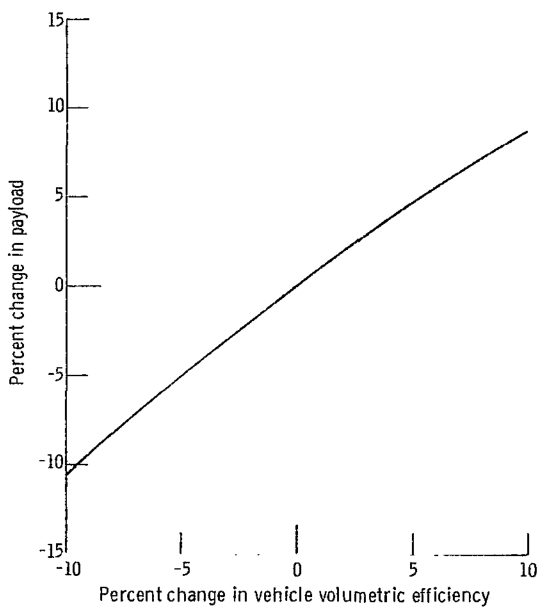

Figure 24. - Effect of vehicle volumetric efficiency on payload. Staging Mach number, 10; rocket-on Mach number, 18; flight path dynamic pressure, 24 kilonewtons per square meter (500 lb/ft^2); stage weight, 227 000 kilograms (500 000 lb); base payload, 23 500 kilograms (51 800 lb).

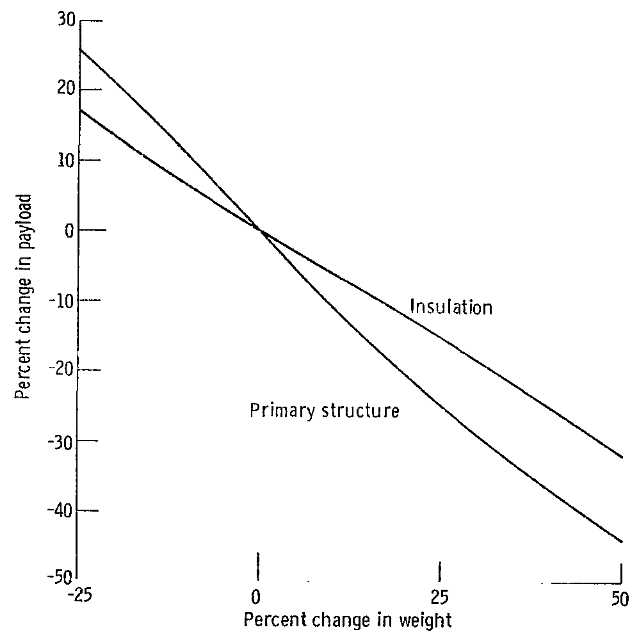

Figure 25. - Effect of primary structure and insulation weights on payload. Staging Mach number, 10; rocket-on Mach number, 18; flight path dynamic pressure, 24 kilonewtons per square meter (500 lb/ft^2); stage weight, 227 000 kilograms (500 000 lb); base payload, 23 500 kilograms (51 800 lb).

CONCLUDING REMARKS

A preliminary mission study was made of a reusable orbital second stage having a propulsion system consisting of separate scramjet and rocket engines. The calculations indicated that for a stage weight of 227 000 kilograms (500 000 lb), a payload of 23 500 kilograms (51 800 lb) or 10.4 percent of stage weight could be delivered into a 500-kilometer (270-n mi) orbit. This was 70 percent higher than the payload of a rocket stage of equal stage weight on the same flight path. When compared with a reusable two-stage shuttle-type rocket vehicle having a payload of 22 700 kilograms (50 000 lb), the total weight at lift-off was reduced 56 percent by using a second stage designed for scramjet-rocket propulsion. In addition, the empty weight was 42 percent lower than for the all-rocket vehicle; thus, a lower cost for hardware (and related items) might be indicated. However, since dynamic pressures normally considered for staging are on the order of 1.2 to 2.4 kilonewtons per square meter (25 to 50 lb/ft^2), the consequences on stage separation dynamics at higher dynamic pressures would have to be investigated. Also, the first-stage hardware weight data used in this study were designed for typical rocket trajectories, and possible structural weight penalties resulting from the different trajectory required for staging at higher dynamic pressures would have to be assessed.

The best payloads were obtained when rocket operation was delayed until about Mach 18 and the scramjet equivalence ratios were scheduled from 1 to 3.85 with increasing Mach number. This fuel-rich schedule was compatible with estimates of scramjet cooling requirements. The performance with stoichiometric equivalence ratios was investigated also, but payloads were lower than those obtained with the fuel-rich schedule. In addition, stoichiometric scramjet-only propulsion did not give sufficient thrust to complete the ascent.

The vehicle configuration featured a flat top, a low angle fore cone and a high angle aft cone boattail which contained the rocket. An annular scramjet wrapped around the underside of the body with the aft cone boattail serving as the exhaust surface. The weight breakdown was about 55 percent propellant, 31 percent structure (which included 8.7 percent for thermal protection and 3.6 percent for equipment), rocket and flyback turbofan engines and crew. Eliminating the flyback turbofans increased the payload by 2.8 percent of stage weight. The planform loadings at the reentry weight were less than the 245 kilograms per square meter (50 lb/ft^2) typical of subsonic lifting body requirements. Since centrifugal effects were large and furnished from 20 to 100 percent of the required lift during ascent, the addition of wings to reduce planform loading seriously degraded the payload due to the added wing weight and drag. The second-stage constant dynamic pressure flight paths that resulted in the best payloads ranged from 24 to 48 kilonewtons per square meter (500 to 1000 lb/ft^2).

This study was intended primarily as an exploratory investigation of the merits of combined scramjet and rocket propulsion for second or orbital stages recognizing that advances in both vehicle and engine technology are required to achieve the attractive payloads presented in this report. In particular, structural weight needs to be more firmly established due to the unique aero-thermo and materials problems of hypersonic vehicles. Advances in scramjet engine technology throughout the flight path from staging to super-orbital velocities are required. High overall contraction ratios, low-loss fuel injection for a wide range of flow rates, good combustion and mixing at high velocities, and good nozzle performance are required. Also, only elementary considerations was given to operational flight problems. A more vigorous optimization of the complete flight path; that is, boost, staging, ascent, trajectory transfer, reentry, and landing should be accomplished.

Lewis Research Center,
National Aeronautics and Space Administration,
Cleveland, Ohio, February 8, 1972,
139-06.

APPENDIX A

SYMBOLS

A_b	vehicle body maximum cross-sectional area
A_c	scramjet cowl cross-sectional area
A_S	scramjet stream tube area
b	vehicle span
b_s	structural span, $(b - 2r_b)/\cos \Lambda_{0.4}$
C_A	axial force coefficient
C_D	vehicle drag coefficient, D/qS_{PL}
$C_{D_{BL}}$	blunt leading edge drag coefficient
C_F	friction drag coefficient
C_L	vehicle aerodynamic lift coefficient, L/qS_{PL}
C_N	normal force coefficient
C_{NEX}	scramjet normal force coefficient
C_p	pressure coefficient
D	drag force
d_s	blunt leading edge diameter
F_{ROC}	thrust of rocket engine
F_{sc}	thrust of scramjet engine
ΔH	fuel enthalpy rise
k	length of cylindrical body section
k_N	nozzle efficiency parameter
L	lift force
l	vehicle length
l_s	length of blunt leading edge
M	flight Mach number
M_{NS}	Mach number normal to shock wave
M_P	pullup Mach number

M_R	rocket-on Mach number
M_S	staging Mach number
M_z	zoom Mach number
n	normal ultimate load factor, 3.0
PR	pressure ratio
p	pressure
$\dot{Q}$	total heat transfer rate
q	dynamic pressure, $(\gamma/2)pM^2$
r	cowl radius
r_b	maximum body radius
r_l	scramjet cowl radius
r_p	payload compartment radius
r_t	representative propellant tank radius
S_P	planform area
S_{PL}	vehicle planform area
S_S	surface area
S_{VF}	planform area of vertical stabilizer
S_W	wing planform area
S_{WF}	body surface area
T_{EQ}	radiation equilibrium temperature
T_{rec}	recovery temperature
t_r	thickness of exposed wing root chord
V	velocity
V_b	volume of body
V_{prop}	volume of propellant
W	weight
W_{body}	structural weight of body
W_{crewc}	weight of crew and consumables
W_{eng}	sum of installed weights of rocket and turbofan engines

W_{equip} combined weight of all fixed equipment (mechanical, electrical, hydraulic, environmental, avionics)

W_{fin} weight of vertical stabilizing surfaces

W_g gross weight at staging

W_{gear} weight of landing gear

W_{MT} empty weight

W_{pay} weight of payload

$W_{p\,\Delta V}$ propellant weight for postorbital maneuvering

W_{PR} propellant weight for rocket

W_{prop} total propellant weight

$W_{P_{SJ}}$ propellant weight for scramjet

$W_{P_{TJ}}$ propellant weight for turbofan

W_R flyback or reentry weight

W_{SJ} weight of scramjet engine

W_{str} structural weight

W_{tank} weight of propellant tanks

W_{TJ} installed weight of flyback turbofan engines

W_{TPS} weight of thermal protection system

W_W weight of wing structure

$W_{W_{90}}$ weight of wing surface that extends maximum planform width to base of body

$\dot{w}_a$ scramjet airflow rate

$\dot{w}_{a_{TJ}}$ turbofan corrected airflow rate

$\dot{w}_f$ hydrogen fuel flow rate

$\dot{w}_r$ rocket propellant flow rate

Z molecular weight ratio

α vehicle angle of attack

β compressibility factor, $\sqrt{|M^2 - 1|}$

γ ratio of specific heats for air

δ deflection angle

ϵ parameter, $M \sin \delta$

η_e ratio of actual to theoretical fuel enthalpy increase by regenerative cooling

θ shockwave angle

Λ sweepback angle

Λ_e effective sweepback angle

$\Lambda_{0.4}$ 40 percent chord sweepback angle

σ cone semiangle

φ scramjet equivalence ratio

φ_c scramjet equivalence ratio for cooling

ψ scramjet central angle

Subscripts:

F fore cone

LE leading edge

R aft or rear cone

W wing

1 representative surface (see sketch (a) in appendix B) - bottom of forebody or semicone

2 representative surface - bottom of wing when present

3 representative surface - vertical stabilizer

4 representative surface - scramjet cylindrical cowl, sides, and body cylindrical surface

5 representative surface - top of body without wing

6 representative surface - top of wing when present

7 tail cone not in exhaust flow

APPENDIX B

AERODYNAMICS, SKIN FRICTION, AND EQUILIBRIUM TEMPERATURE ANALYSIS

The specified configuration was represented by the seven flow regions depicted in sketch (a). The force coefficients for each region were determined. In addition the descriptive lengths or mean-aerodynamic chords for each region were used for the friction and radiation equilibrium temperature calculations. (Symbols are defined in appendix A.) For purposes of brevity the seven regions are assigned the following numbers by which they will be identified in the following discussion:

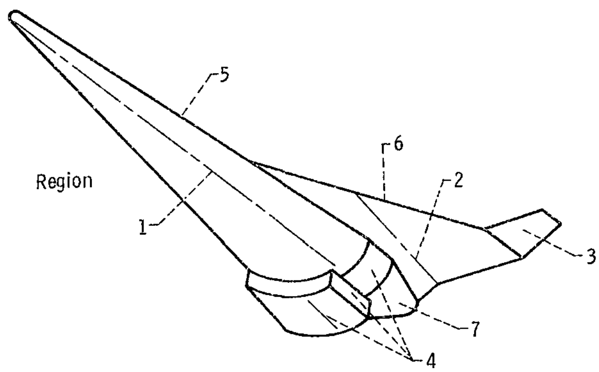

(a)

(1) Bottom of forward semicone

(2) Bottom of wing

(3) Vertical stabilizer

(4) Scramjet cylindrical cowl and sides and body cylindrical surface

(5) Top of body without wing

(6) Top of wing

(7) Aft cone not in scramjet exhaust flow

Aerodynamics

The vehicle angle of attack varies from positive to negative values along the lifting trajectory as mass decreases and centrifugal lift increases. When the various regions are in compression, Newtonian impact theory is used to calculate the pressure forces.

For expansion flow fields the pressure forces are determined by Van Dyke's unified pressure coefficient for pressures greater than zero. The normal and axial compression force coefficients for the bottom portion of the forward semicone referenced to the semicone base area were derived from the methods of reference 21 and are as follows:

$$C_{N_1} = \frac{4}{\pi} \cot \sigma_F \left(A + \frac{\pi}{8} B + \frac{2}{3} C \right) \qquad \alpha > 0, \ \alpha > -\sigma_F \tag{B1}$$

$$C_{A_1} = \left(2A + \frac{2}{\pi} B + C \right) \qquad \alpha > -\sigma_F \tag{B2}$$

where

$$A = \cos^2 \alpha \sin^2 \sigma_F$$

$$B = \sin 2\alpha \sin 2\sigma_F$$

$$C = \sin^2 \alpha \cos^2 \sigma_F$$

The bottom of the forward semicone did not encounter expansion flow conditions since negative angles of attack did not exceed the semicone angle. Compressive force coefficients for the body and wing upper surfaces (regions 5 and 6) at negative angles of attack and wing lower surfaces (region 2) at positive angles of attack were determined from Newtonian theory assuming flat plate pressure coefficients (ref. 22)

$$C_{N_{2,5,6}} = 2 \sin^2 \alpha \tag{B3}$$

where C_N is referenced to the individual planform area of each region.

The normal force coefficient for expansion flow fields for the vehicle and wing tops at positive angles of attack and wing bottom at negative angles of attack were evaluated by Van Dyke's small disturbance theory pressure coefficient:

$$C_{N_{2,5,6}} = C_p = \alpha^2 \left[\frac{\gamma + 1}{2} - \sqrt{\left(\frac{\gamma + 1}{2} \right)^2 + \frac{4}{\beta^2 \alpha^2}} \right] \tag{B4}$$

The scramjet cowl was assumed to be alined with the vehicle axis resulting in a zero axial force coefficient. The normal force coefficient referenced to the cowl cross section area, $\pi/2r_l^2$, is given by

$$C_{N_4} = \frac{1.4}{\pi r_l} k \sin^2 \alpha \sin \frac{\psi}{2} \left(\cos^2 \frac{\psi}{2} + 2\right) \tag{B5}$$

Blunt leading edges were assumed for the vertical stabilizer, scramjet cowl lip, and wing leading edge. The following relation from reference 21 for a circular cylinder in Newtonian flow was used for the bluntness drag coefficients:

$$C_{D_{BL}} = \frac{4.8}{\pi d_s} l_s \cos^3 \Lambda_e \tag{B6}$$

The diameter of each leading edge d_s was assigned, whereas the length was calculated from geometry. The effective sweepback angle is equal to the geometric sweepback angle for the wing, zero for the scramjet cowl, and equal to the geometric angle plus the angle of attack for the vertical stabilizer.

Skin Friction and Equilibrium Temperatures

Since the flow deflection angles on the forward semicone and scramjet cowl surfaces are not uniform at angles of attack, average or representative deflection angles were determined to reduce the complexity of the skin friction and radiation equilibrium temperature analysis for these surfaces. The representative deflection angle for the bottom of the forward semicone was prescribed as the average between the bottom centerline and the side

$$\delta_1 = \sigma_F + \frac{\alpha}{2} \qquad \alpha > -\sigma_F \tag{B7}$$

For the scramjet cowl, which may have an included angle ψ of less than 180°, the mean deflection angle was taken as

$$\delta_4 = \alpha - \frac{\alpha}{2}\left(\frac{\psi}{180}\right) \tag{B8}$$

This tacitly assumes that the semicone shock uniformly intercepts the cowl lip. For the surfaces 2, 3, 5, and 6

$$\delta = \alpha \tag{B9}$$

Thus, the vertical stabilizer surface 3 is analyzed as in the angle of attack plane. The purpose of this is to build in a thermal protection system for possible maneuvers. For surface 7, the aft cone not in exhaust flow, the deflection angle was assumed equal to the aft cone angle, if such an expansion did not give negative pressure ratio; that is,

$$\delta_7 = -\sigma_R \tag{B10}$$

When the individual deflection angle was positive, indicating a flow compression, the Mach number normal to the shock wave was determined by means of the following approximate equations (ref. 23):

For cone flow (surface 1)

$$M_{NS} = M \sin \theta \sim 2\left(\frac{\gamma + 1}{\gamma + 3}\right)\epsilon + \exp\left[-2\left(\frac{\gamma + 1}{\gamma + 3}\right)\epsilon\right] \tag{B11}$$

where $\epsilon = M \sin \delta_1$. For regions 2, 3, 5, and 6, assuming wedge or two-dimensional flow results in

$$M_{NS} = M \sin \theta \sim \left(\frac{\gamma + 1}{2}\right)\epsilon + \exp\left[-\left(\frac{\gamma + 1}{4}\right)\epsilon\right] \tag{B12}$$

For either case, then, the local flow properties such as density, temperature, velocity, and pressure ratios were determined from the usual constant gamma oblique shock relations (ref. 24) using the approximation to $M \sin \theta$. In general the level of compressibility ($Z < 1.02$) was less than 2 percent and real gas relations are not needed for these functions.

In a similar manner the local flow properties for expansion regions can be found once the pressure ratio is obtained from the pressure coefficient defined by equation (B4):

$$PR = 1 + \frac{\gamma}{2} M^2 C_p \tag{B13}$$

When $PR = 0$, the wall temperature of that particular surface was arbitrarily set at 555 K. Using the flow properties thus determined local skin friction coefficients and equilibrium temperatures were calculated along the descriptive length or mean aerodynamic chord of each region. Since Reynold's numbers 3 meters (10 ft) aft of the nose were in excess of 10^7, a turbulent boundary layer was assumed. Eckert's reference enthalpy technique was used with the skin friction relation given in reference 23. Enthalpies for the recovery and wall temperatures were approximated by real gas relations given in reference 25. The real gas recovery temperatures for the flight paths of interest were estimated by the following relation:

$$T_{rec} = \frac{5}{9} \exp\left(8.84 + \frac{M - 10}{9}\right) \text{ (K)}$$

or (B14)

$$T_{rec} = \exp\left(8.84 + \frac{M - 10}{9}\right) \text{ (}^{o}\text{R)}$$

An emissivity of 0.8 was assumed in determining the equilibrium temperatures. At the shoulder of the blunt leading edge of each region the following values were assigned in order to simulate some initial run of laminar flow:

Friction coefficient	0.0005
Heat transfer coefficient, $J/(m^2)(sec)(K)$; $Btu/(ft^2)(sec)(^{o}R)$	1.9; 0.0003
Equilibrium temperature	Greater than next downstream temperature given by $T_{EQ_1} = 11\,M + T_{EQ_2}$ (K) or $T_{EQ_1} = 20\,M + T_{EQ_2}$ (^{o}R)

The average skin friction coefficient and radiation equilibrium temperature for each panel were then obtained by numerical integration of the local values over the representative length or mean-aerodynamic chord.

The overall vehicle skin friction coefficient was then determined by

$$C_F = C_{F_1}\frac{S_{S_1}}{S_{PL}} + C_{F_2}\frac{S_{P_2}}{S_{PL}} + C_{F_3}\frac{S_{P_3}}{S_{PL}} + C_{F_4}\frac{S_{S_4}}{S_{PL}} + C_{F_5}\frac{S_{P_5}}{S_{PL}} + C_{F_6}\frac{S_{P_6}}{S_{PL}} + C_{F_7}\frac{S_{S_7}}{S_{PL}} \tag{B15}$$

Overall Force Coefficients

The overall pressure-force coefficients based on planform area are

$$C_N = \frac{\pi}{2}\frac{r_b^2 C_{N_1}}{S_{PL}} + C_{N_2}\frac{S_{P_2}}{S_{PL}} + C_{N_4}\frac{\frac{\pi}{2} r_l^2}{S_{PL}} + C_{N_5}\frac{S_{P_5}}{S_{PL}} + C_{N_6}\frac{S_{P_6}}{S_{PL}} + C_{NEX}\frac{\pi r_b^2}{S_{PL}} \tag{B16}$$

$$C_A = \frac{\pi}{2} r_b^2 \frac{C_{A_1}}{S_{PL}} \tag{B17}$$

Converting to lift and drag coefficients yields:

$$C_L = C_N \cos \alpha - C_A \sin \alpha \tag{B18}$$

$$C_D = C_A \cos \alpha + C_N \sin \alpha + C_F + C_{D_{BL_2}} + C_{D_{BL_3}} + C_{D_{BL_4}} \tag{B19}$$

APPENDIX C

WEIGHT ESTIMATING PROCEDURES

The vehicle weight statements adopted for this study are outlined herein. (Symbols are defined in appendix A.)

The gross weight of the upper stage at staging was

$$W_g = W_{MT} + W_{prop} + W_{pay} + W_{crewc} \tag{C1}$$

where the empty weight

$$W_{MT} = W_{str} + W_{eng} + W_{equip} \tag{C2}$$

and the total propellant weight,

$$W_{prop} = W_{P_{TJ}} + W_{PR} + W_{P_{SJ}} + W_{p\ \Delta V} \tag{C3}$$

The two man crew plus six days consumables is

$$W_{crewc} = 317.4 \text{ kg } (700 \text{ lb}) \tag{C4}$$

The payload W_{pay} is of course the derived result from equation (C1).

The equipment weight W_{equip} in equation (C2), includes the combined weight of all fixed equipment (mechanical, electrical, hydraulic, environmental, and avionics) and is determined from

$$W_{equip} = 4536 + 10^{-2}(W_g - 0.136\times10^6) \text{ (kg)}$$

or (C5)

$$W_{equip} = 10^4 + 10^{-2}(W_g - 0.3\times10^6) \text{ (lb)}$$

The engine weight term W_{eng} includes the rocket and flyback turbofans but not the scramjet which is included in the structural weight.

The structural weight is defined as

$$W_{str} = W_{body} + W_{fin} + W_{gear} + W_{tank} + W_{SJ} + W_{W} + W_{TPS} \tag{C6}$$

Notice that the thermal protection system weight is a separate item. The various terms of equation (C6) are then evaluated.

The body primary weight is given as

$$W_{body} = 6.1(1.2\ S_{WF} + V_b)\ \text{(kg)}$$

or (C7)

$$W_{body} = 1.5(S_{WF} + 0.38\ V_b)\ \text{(lb)}$$

using the procedure of reference 26 for blended bodies.

The vertical stabilizer weight is estimated as a function of the surface area

$$W_{fin} = 39.0\ S_{VF}\ \text{(kg)}$$

or (C8)

$$W_{fin} = 8.0\ S_{VF}\ \text{(lb)}$$

Assuming the flyback or landing weight will be about 38 percent of the initial stage weight, the landing gear weight is

$$W_{gear} = 0.016\ W_g \tag{C9}$$

Assuming an ullage allowance of 10 percent, the tank weight for the LH_2 and LOX is calculated from the following equation:

$$W_{tank} = 22.76\ \frac{V_{prop}}{(r_b - r_p)}\ \text{(kg)}$$

or (C10)

$$W_{tank} = 4.66\ \frac{V_{prop}}{(r_b - r_p)}\ \text{(lb)}$$

For this relation the surface to volume ratio of the average or representative propellant tanks is $4.66/r_t$ and the tank weight (including sufficient internal insulation to limit boil-off and heat soak is 4.9 kilograms per square meter (1 lb/ft^2). The representative propellant tank diameter is the difference between the body maximum radius and the payload envelope radius $r_b - r_p$.

The scramjet is composed of a cowl and side panels between the cowl and vehicle body. These have a primary structural backbone with a thermal protection of insulation and metal shingles on the external surface and regenerative cooling panels on the scramjet gas side. The vehicle centerbody and boattail in scramjet flow are also regeneratively cooled. The cowl primary structure is hoop stressed for steel-type material at a stress level of 172.4×10^6 newtons per square meter (25×10^3 $lb/in.^2$) compatible with a metal temperature of 1000 K (1800° R) for 100 hours and the highest internal pressures experienced along the flight path. The side panels were analyzed as panels in tension and bending for the same environmental conditions as the cowl. For weight estimating purposes, the cowl length includes a 1.83-meter (6-ft) combustor corresponding to estimated mixing and reaction lengths at orbital velocities plus one-fourth of the vehicle aft semicone length.

A unit weight of 11.2 kilograms per square meter (2.29 lb/ft^2) (ref. 12) was assumed for the regenerative cooling panels for a metal temperature of 1000 K (1800° R). The exterior surface heat protection system weight is described later.

The weight of the wing primary structure is based on the following simple correlation

$$W_W = 642.5\left(\frac{23.75}{10^9} W_g n b_s \frac{S_W}{t_r}\right)^{0.64} + W_{W_{90}} \quad \text{(kg)}$$

or (C11)

$$1420\left(\frac{W_g n b_s}{10^9} \frac{S_W}{t_r}\right)^{0.64} + W_{W_{90}} \quad \text{(lb)}$$

where the primary structural weight refers to a complete conventional wing without thermal protection. The exponential term of the equation is attributed to R. L. Benson of the Convair Division of General Dynamics. The planform with a sweepback of 90° results in a horizontal surface addition which extends the planform maximum width to the end of the body. The weight of this surface $W_{W_{90}}$ is taken as 39.0 kilograms per square meter (8 lb/ft^2).

The thermal protection system was selected as a metallic shingle with backside insulation. The blunt leading edges are not considered as a separate weight item. The thermal protection system weight was calculated for the average equilibrium surface temperature for each of the seven flow regions described in appendix B. The unit weight of the metallic shingle including corrugated stiffening and local supports was uniformly taken as 6.8 kilograms per square meter (1.4 lb/ft^2) (ref. 11). The peak average surface temperature was generally high enough to require the use of refractory alloys such as niobium or tantalum. The insulation thicknesses were computed from a one-dimensional transient heat conduction analysis. The insulation material assumed was Dynaquartz with a density of 104 kilograms per square meter (6.5 lb/ft^3) with a prescribed backside temperature of 367 K (660° R). The scramjet cowl and side panel external surfaces had an insulation backside temperature of 1000 K (1800° R) compatible with the regeneratively cooled structure.

REFERENCES

1. Anon.: Space Shuttle. Vol. 2: Final Vehicle Configurations. Rep. GDC-DCB69-046-Vol. 2, General Dynamics/Convair (NASA CR-102550), Oct. 31, 1969.

2. Anon.: Study of Integral Launch and Reentry Vehicle System. Vol. 2: Technology Development. Rep. SD-69-573-2, North American Rockwell Corp. (NASA CR-102106), Dec. 1969.

3. Anon.: A Two-Stage Fixed Wing Space Transportation System. Vol. I: Condensed Summary. Rep. MDC-E0056, Vol. 1, McDonnell-Douglas Astronautics Co. (NASA CR-102086), Dec. 1969.

4. Escher, William J. D.; Flornes, Bruce J.; and Frank, Harry: Results of a Study of Composite Propulsion Systems for Advanced Launch Vehicle Applications. Presented at AIAA Second Propulsion Joint Specialist Conference, Colorado Springs, Colo., June 13-17, 1966.

5. Anon.: Technologies and Economics of Reusable Space Launch Vehicles. Volume I: Summary and Conclusions. Report R-114-Vol. 1, Institute for Defense Analyses, Feb. 1966. (Available from DDC as AD-374488L.)

6. Lockheed California Company: Study of Advanced Airbreathing Launch Vehicles With Cruise Capability, Report LR20692 LAC/614885 12 May 1967. Contract NAS2-4084.

7. Gregory, Thomas J.; Williams, Louis J.; and Wilcox, Darrell E.: The Airbreathing Launch Vehicle for Earth Orbit Shuttle - Performance and Operation. Paper 70-270, AIAA, Feb. 1970.

8. Knip, Gerald, Jr. and Eisenberg, Joseph D.: Performance Estimates for Space Shuttle Vehicles Using a Hydrogen or a Methane-Fueled Turboramjet-Powered First Stage. NASA TN D-6634, 1972.

9. Mager, A.: Cost Effectiveness of Scramjet as a Second Stage in Space Boosting Applications. Rep. TOR-669(6520-95)-1, Aerospace Corp., Nov. 1965.

10. Dobrowolski, Andrzej; and Allen, John L.: Conceptual Study of Rocket-Scramjet Hybrid Engines in a Lifting Reusable Second Stage. NASA TN D-5218, 1969.

11. Guyton, Robert G.; and Ingram, Jesse C., Jr.: Structures and Materials Assement for Hypersonic Vehicle Technology. Universal Technology Corp. (AFFDL-TR-69-83, AD-864714), Nov. 1969.

12. Jensen, Roger: Weight Estimation of Hypersonic Inlets. Paper 655, Society of Aeronautical Weight Engineers, May 1968.

13. Kraft, Gerald A.; and Whitlow, John B., Jr.: Design Point Study of Auxiliary Airbreathing Engines for a Space Shuttle. NASA TM X-52810, May 1970.

14. Anon.: Study of Integral Launch and Reentry Vehicle System. Vol. 4: Technical Report, Phase 2: Design and Subsystems Analysis. Rep. SD-69-573-4, North American Rockwell Corp. (NASA CR-102105), Dec. 1969.

15. Sasman, Philip K.; and Cresci, Robert J.: Compressible Turbulent Boundary Layer with Pressure Gradient and Heat Transfer. AIAA J., vol. 4, no. 1, Jan. 1966, pp. 19-25.

16. Franciscus, Leo, C.; and Healy, Jeanne A.: Computer Program for Determining Effects of Chemical Kinetics on Exhaust-Nozzle Performance. NASA TN D-4144, 1967.

17. Franciscus, Leo C.: Off-Design Performance of Hypersonic Supersonic Combustion Ramjets. Presented at the AIAA 1st Annual Meeting, Washington, D.C., June 29-July 2, 1964.

18. Franciscus, Leo C.; and Lezberg, Erwin A.: Effects of Exhaust Nozzle Recombination on Hypersonic Ramjet Performance: II - Analytical Investigation. AIAA J., vol. 1, no. 9, Sept. 1963, pp. 2077-2083.

19. Anon.: Flight Test Results Pertaining to the Space Shuttlecraft. NASA TM X-2101, 1970.

20. Gorsuch, Paul D.: Tanzilli, Richard C.; Florence, Dwight E.; and Gluck, Robert: Development of Non-Metallic External Insulation Thermal Protection Systems for Space Shuttle. Paper 700771, SAE, Oct. 1970.

21. Grimminger, G.; Williams, E. P.; and Young, G. B. W.: Lift on Inclined Bodies of Revolution in Hypersonic Flow. J. Aeron. Sci., vol. 17, no. 11, Nov. 1950, pp. 675-690.

22. Truitt, Robert W.: Hypersonic Aerodynamics. Ronald Press Co., 1959.

23. Gentry, Arvel E.: Hypersonic Arbitrary-Body Aerodynamic Computer Program, Mark III Version. Rep. DAC-61552, Douglass Aircraft Corp., Apr. 1968. (Available from DDC as AD-851811.)

24. Ames Research Staff: Equations, Tables, and Charts for Compressible Flow. NACA Rep. 1135, 1953.

25. Hansen, C. Frederick: Approximations for the Thermodynamic and Transport Properties of High-Temperature Air. NASA TR R-50, 1959.

26. Thompson, W. R.: Weight and Size Analyses of Advanced Cruise and Launch Vehicles. Vol. I: Final Technical Report and Data Handbook. Rep. GDC-DCB-66-008, Vol. 1, General Dynamics/Convair (NASA CR-89451), Feb. 1966.

NASA-Langley, 1972 —— 28 E-6555

NATIONAL AERONAUTICS AND SPACE ADMISTRATION
WASHINGTON, D.C. 20546

OFFICIAL BUSINESS
PENALTY FOR PRIVATE USE $300

FIRST CLASS MAIL

POSTAGE AND FEES PAID
NATIONAL AERONAUTICS AND
SPACE ADMINISTRATION

U.S.MAIL

019 001 C1 U 28 720505 S00903DS
DEPT OF THE AIR FORCE
AF WEAPONS LAB (AFSC)
TECH LIBRARY/WLOL/
ATTN: E LOU BOWMAN, CHIEF
KIRTLAND AFB NM 87117

POSTMASTER: If Undeliverable (Section 158 Postal Manual) Do Not Return

"The aeronautical and space activities of the United States shall be conducted so as to contribute . . . to the expansion of human knowledge of phenomena in the atmosphere and space. The Administration shall provide for the widest practicable and appropriate dissemination of information concerning its activities and the results thereof."

—NATIONAL AERONAUTICS AND SPACE ACT OF 1958

NASA SCIENTIFIC AND TECHNICAL PUBLICATIONS

TECHNICAL REPORTS: Scientific and technical information considered important, complete, and a lasting contribution to existing knowledge.

TECHNICAL NOTES: Information less broad in scope but nevertheless of importance as a contribution to existing knowledge.

TECHNICAL MEMORANDUMS: Information receiving limited distribution because of preliminary data, security classification, or other reasons.

CONTRACTOR REPORTS: Scientific and technical information generated under a NASA contract or grant and considered an important contribution to existing knowledge.

TECHNICAL TRANSLATIONS: Information published in a foreign language considered to merit NASA distribution in English.

SPECIAL PUBLICATIONS: Information derived from or of value to NASA activities. Publications include conference proceedings, monographs, data compilations, handbooks, sourcebooks, and special bibliographies.

TECHNOLOGY UTILIZATION PUBLICATIONS: Information on technology used by NASA that may be of particular interest in commercial and other non-aerospace applications. Publications include Tech Briefs, Technology Utilization Reports and Technology Surveys.

Details on the availability of these publications may be obtained from:

SCIENTIFIC AND TECHNICAL INFORMATION OFFICE

NATIONAL AERONAUTICS AND SPACE ADMINISTRATION

Washington, D.C. 20546